IEEE TRANSACTIONS ON
VEHICULAR TECHNOLOGY
A PUBLICATION OF THE IEEE VEHICULAR TECHNOLOGY SOCIETY

IEEE Xplore® Digital Library
http://ieeexplore.ieee.org/Xplore

Global Trends in High-Power On-Board Chargers for Electric Vehicles

Alireza Khaligh, *Senior Member, IEEE*, and Michael D'Antonio, *Student Member, IEEE*

***Abstract* — This manuscript provides a comprehensive review and analyses on the state-of-the-art and future trends for high-power conductive onboard chargers for electric vehicles. To provide a global context, a summary of global charging standards and EV related trends are presented, which demonstrates momentum towards higher power rating on-board chargers (OBCs). High-power OBCs are either unidirectional or bidirectional, and have either an integrated or non-integrated system architecture. Non-integrated high-power OBCs are studied from both industry and academia, and the former are used to illustrate the current state-of-the-art. The latter are classified based on the converter design approach, studied for their principle of operation, and compared over power density, weight, efficiency, and other metrics. In addition to non-integrated OBCs, recent advancements in propulsion-machine integrated OBC solutions are also presented. Other integrated OBC techniques are also discussed which include system integration with the EV's auxiliary power module and wireless charging systems. Finally, future charging strategies and functionalities in charging infrastructures are addressed, and global OBC trends are summarized.**

***Index Terms* — Electric vehicles, on-board chargers, conductive charging, wireless charging, integrated chargers, smart charging, grid-to-vehicle, vehicle-to-grid, charging infrastructure, power electronics.**

I. Introduction

The growing popularity of battery electric vehicles (BEVs) and plug-in hybrid electric vehicles (PHEVs), commutatively called electric vehicles (EVs), can be attributed to several significant benefits, such as reduced global greenhouse gas (GHG) emissions [1], and superior vehicular performance [2], while progressing towards cost competitiveness with internal combustion engine (ICE) vehicles in the mid-to-late 2020s due to plunging lithium-ion battery costs [3],[4].

Due to the rapid growth in EV sales, totaling 3.1 million units as of the end of 2017 [6], many countries have begun to issue and express interest in mandates regarding the future of vehicle sales, including the United States (US), China, India, and many countries within the European Union. In the US, the state government of California has declared a Zero Emission Vehicle (ZEV) mandate as of 2016, which requires automakers in the state to sell an increasing amount of ultra-low or zero-emission vehicles year over year [5],[6]. This mandate was later adopted by nine other US states [6]. Based on California's ZEV mandate, China issued their New Energy Vehicle (NEV) mandate, which became effective as of April 2018 [6]. India on the other hand has drafted and released a roadmap towards only EV sales by 2047 [6]. Similarly, several countries in the European Union (EU), including Finland, Ireland, Netherlands, and Norway, are continually developing their future targets for EV sales [5],[6]. However, as EVs become more widespread it is critical for both chargers and global power system infrastructures to be prepared for the large influx of concentrated energy demand.

The trend of increasing power in OBCs is evident as early EVs were charged in power levels around 3.3 kW [7],[8], however currently nearly every EV has provisions for 6.6 kW, 7.4 kW, and 11 kW OBCs, with additional significantly higher-power off-board charging compatibilities. The trend is predominantly influenced by the increase in EV battery capacity, which was necessary to alleviate range anxiety and improve vehicle capabilities. While the current state of high-power charging technology is primarily realized with off-board chargers, the presence of a high-power OBC will provide consumer convenience, with utilities simply offering high-power AC inputs as opposed to conditioned DC fast-charging inputs. However, as EV OBC power ratings continue to increase, new challenges are presented in terms of compact, lightweight and efficient OBC solutions. Compact charging technologies are especially important in the automotive industry, as the OBC needs to fit amongst the multitude of other components within the EV.

Aside from benefits to charging time and the fast-charging infrastructure, increased power level OBCs will help utility companies incorporate more smart features to the electric grid. For instance, bidirectional OBCs will enable smart vehicle-to-grid (V2G) functionalities, such as peak shaving and frequency regulation. Furthermore, bidirectional OBCs would allow consumers to use their EV's stored energy for other purposes, for instance supplying vehicle-to-home (V2H) power during grid outages.

The envisioned typical EV drivetrain and associated charging methods are presented in Fig. 1. As shown, the major power electronics systems on-board an EV includes the OBC, auxiliary power module (APM), motor drive inverter, and optional wireless charger. EV battery charging methods include on-board charging with the OBC and APM, off-board charging, and wireless charging, which can be alternatively categorized as either conductive (on-board and off-board charging) or inductive (wireless charging). The wireless charging system has been depicted as an optional interface,

Digital Object Identifier 10.1109/TVT.2019.2897050

because wireless charging systems have not yet been implemented in EVs by industry. While future EVs may only have either conductive or inductive charging interfaces, it is envisioned that EVs may have both interfaces in the near future for interoperability, and charging compatibility away from home. This manuscript presents various structures currently utilized and researched for high-power (>7.4 kW) conductive OBC enablement.

There are two main categories for high-power OBC systems: non-integrated and integrated. Non-integrated OBC systems designate that the OBC is a standalone unit with a singular functionality to serve as the EV's propulsion battery charger. On the other hand, integrated OBC systems designate that additional power electronics systems and functionalities are integrated with the OBC. One example of an integrated solution is the propulsion machine integrated OBC, which serves to reuse the high power-rated electrical machine and motor-drive inverter to facilitate propulsion battery charging when the vehicle is not running. Another example of an integrated OBC solution combines the OBC and APM into a single topology. Several other examples of integrated OBC systems will be examined in this manuscript.

The structure of this manuscript is as follows: Section II provides background on currently utilized OBCs in global EVs, global EV power-level classifications, charger directionality, and the identification of several key trends in EVs and OBCs. Based on the identified trends, Section III discusses and categorizes high-power non-integrated OBC solutions used both in industry as well as research institutions. Aside from the non-integrated OBC study, Section III analyzes potential converter candidates for the AC-DC and DC-DC stages of a two-stage OBC, and presents two novel structures for propulsion-machine integrated OBCs. In Section IV, global charging infrastructures are evaluated, and future charging strategies as well as the capabilities of OBCs in the electric infrastructures are introduced. Finally, Section V provides a discussion of the future trends in device utilization and converter integration, alongside a summary of the trends identified throughout the manuscript.

II. Background

A. Popular EV Specifications

Globally, 95% of EV sales are taking place in just ten countries, namely the US, China, Japan, Canada and six European countries (Norway, UK, France, Germany, Netherlands, and Sweden) [9]. According to [10], Table I identifies the most popular fully electric vehicles in Europe, the US, and China, and compares them based on their motor rating, battery capacity, range, and OBC power rating. It is evident that the motor ratings for most EVs are between 30 kW and ~200 kW. Furthermore, EVs in Europe and the US tend to have a larger battery capacity and thus longer-range capability than those sold in China, likely due to range anxiety and limited charging station deployment. Most importantly, every popular EV throughout the world currently utilizes a level-2 OBC between 6.6 kW and 7.4 kW, which represents a doubling in level-2 OBC power levels from early EVs shown in [7].

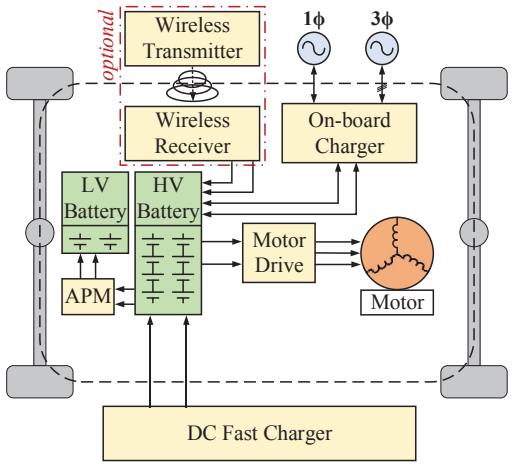

Fig. 1. Envisioned typical EV power system and charging modes.

B. Classification of EV Chargers

OBCs are designed as stand-alone units that communicate with an electric vehicle supply equipment (EVSE) and the vehicle's battery management system (BMS), to deliver the requested charging voltage and current to the EV's high-voltage propulsion battery. Therefore, an important part of the charging process is for the BMS to interpret the correct state of charge (SoC) of the battery and for the charger to deliver the correct charging profile. A review on SoC estimation methods was recently published in [26], and battery voltage equalizer circuits are studied in [27]. Furthermore, the OBC in charging mode needs to ensure that power quality standards are met on the grid-side. The US, European, and Chinese standards regarding harmonic injection for EV chargers in charging mode are addressed in the Society of Automotive Engineers (SAE) J2894 [28], International Electrotechnical Commission (IEC) 61000 [29], Guobiao recommended standards (GB/T) 14549 [30], and IEEE 519 [31]. Galvanic isolation is a requirement in majority of EV OBC systems per safety standards including Underwriters Laboratories (UL) 2202 and IEC 60950 [32]. On the other hand, if EVs operate as a source and the OBC is utilized to regulate external power flow, the OBC should comply with the microgrid inverter standards, detailed in IEEE 1547 [33], IEEE 2030 [34], IEC 62109 [35], UL 1741 [36], and NB/T 33015 [37]. As operation modes regarding EVs as an energy source become more mature, it may be necessary to pose more stringent and well-defined standards.

EV OBCs are categorized as level-1, level-2, and level-3 chargers based on their power levels according to SAE J1772 standard [38]. On the other hand, EVSE interface connectors are based on SAE J1772 in the US [38], the IEC 62196 standard in Europe [39], and GB/T 20234 standard in China [40]. The ratings of commercially available interface plugs for charging levels are retrieved from either Phoenix Contact [41], or the respective standard.

TABLE I
GLOBAL EV SPECIFICATIONS

	EV Model	Motor Rating [kW]	Battery Capacity [kWh]	Range [mi]	OBC Rating [kW]
Europe	Smart Fortwo ED [11]	55	17.6	58	7.2
	Hyundai Ioniq Elec. [12]	88	28	110	6.6
	Kia Soul EV [13]	81	30	110	6.6
	Renault Zoe [14]	80	41	250	43
	VW e-Golf [15]*	100	35.8	125	7.2
	BMW i3 [16]*	125	33	114	7.4
	Nissan Leaf [17]*	110	40	151	6.6
US	Tesla Model 3 [18],[19]	192	75	220	11.5
	Chevy Bolt [20]	150	60	238	7.2
	Ford Focus Electric [21]	107	33.5	115	6.6
China	BAIC EC180 [22]	30	22	101	Level-2
	Chery eQ [23]	30	32	157	Level-2
	JAC iEV7 S/E [24]	50	24	125	Level-2
	JMC E200 [25]	30	17.3	95	Level-2

also best seller in USA market

1) Level-1: Level-1 EV chargers have the lowest charging power level, and hence take the longest time to achieve full battery charge. The peak power of AC level-1 chargers is 3.7 kW [6],[38]. In the United States, plug options for level-1 charging include the J1772 Type 1 EVSE displayed in Fig. 2(a) [38],[41]. In Europe and China, plug options are conventional outlets that are not typically utilized for EV charging [6], and thus they are excluded from this discussion.

2) Level-2: Level-2 EV chargers have growing popularity within the EV community on a global scale. The peak power of level-2 chargers is 22 kW [6],[38]. As seen in Table I, almost every popular EV worldwide utilizes level-2 OBCs in the 6.6 kW-7.4 kW range. This power level is most suitable for current battery capacities, because full battery charging can be nearly completed in an overnight charging session (7-10hrs). Level-2 charging in the US can be realized with an SAE J1772 Type 1 EVSE shown in Fig. 2(a) [38],[41], or the proprietary Tesla plug. In Europe, level-2 charging is achieved with the IEC62196-2 Type 2 plug, seen in Fig. 2(b) [39],[41]. Finally, in China the GB/T 20234 AC plug is utilized for level-2 charging [40],[41]. The GB/T 20234 AC plug is not shown in Fig. 2, as it is derived from the IEC62196-2 Type 2 plug.

3) Level-3 AC: Level-3 EV chargers are the highest charging power options. Level-3 AC-chargers provide three-phase AC for power levels between 22 kW and 43.5 kW [6],[38]. Level-3 AC-chargers can be on-board the vehicle, which is the case for the Renault Zoe propulsion-integrated OBC [14], and the Continental AllCharge system [42]. A three-phase AC plug standard is currently being developed in the US, titled SAE J3068 [6],[43]. Level-3 AC-chargers are realized in Europe by the IEC 62196-2 Type 2 plug [39],[41], and in China by the GB/T 20234 AC plug [40],[41].

4) Level-3 DC: Level-3 DC-chargers provide direct power to the EV's battery for power levels up to 350 kW, or higher [44],[45]. Due to their high-power level and hence bulky size, level-3 DC-chargers are located off-board the EV. DC level-3 is the fastest charging option, which for Extreme Fast Charging (XFC) is proposed to achieve 200 additional miles of driving range in 10 minutes or less [44],[45]. However, the development of a ubiquitous high-power off-board charging infrastructure will take significant time as well as a substantial monetary investment. In the United States, the CCS Combo 1 plug shown in Fig. 2(c) [38],[39],[41], the CHAdeMO shown in Fig. 2(f) [39], and the Tesla supercharger shown in Fig. 2(h) are utilized for DC level-3 charging. In Europe, DC level-3 plugs include the CCS Combo 2 shown in Fig. 2(d) [39],[41], the CHAdeMO, and Tesla supercharger. Finally, DC level-3 charging in China is realized with the GB/T 20234 DC plug shown in Fig. 2(g) [40],[41].

The SAE J1772, IEC62196 Type 2, GB/T20234-3, SAE/IEC DC Combos, CHAdeMO, and Tesla male plugs can be seen in Fig. 2(a)-(h), with their connection ports identified. The connection ports utilized are defined as AC Line A/B/C (L1/2/3), Neutral (N), Connection Switch (CS), Control Pilot (CP), Protected Earth (PE), Proximity Pilot (PP), DC Input (DC±), Ground (GND), Controller Area Network (CAN-H/L), Auxiliary Power Supply (aux±), Proximity Detection (PD), and Not Connected (NC). The discussion presented on EV charger classifications is summarized in Table II, and the various plug types and their respective ratings are summarized in Table III. It is clear that there are many different charging standards, and perhaps interoperability could help move the industry further at a faster rate.

C. Unidirectional and Bidirectional EV Chargers

EV OBC systems can either support unidirectional or bidirectional power flow, as indicated by the arrows in Fig. 1, each with distinct advantages and disadvantages. EV manufacturers may currently be reluctant to incorporate bidirectional OBCs due to concerns about increased OBC cost and volume, and battery degradation. Additionally, while some current EV OBCs may be compatible with bidirectional power flow, this feature has primarily gone unutilized as utility companies have yet to implement the complementary smart power system architecture. However, it is widely believed that bidirectional chargers will be more prevalent in future OBCs.

1) Unidirectional Chargers: The typical structure of a unidirectional charger is shown in Fig. 3(a). To reduce system complexity, the front-end and DC-DC secondary side after isolation are typically realized using diode bridges. However, there are several unidirectional chargers that at least use an active front-end. Benefits of an active front-end power factor correction (PFC) stage in unidirectional chargers includes a reduction in total PFC circuit components in the conduction path leading to higher efficiency, and enhanced functionality such as adjustable power factor control. Advantages of unidirectional chargers are reduced system complexity, fewer active circuit components, thus reduced system cost, and compact size. However, their profound disadvantage lies in the inability to facilitate the future of advanced smart grid functionalities.

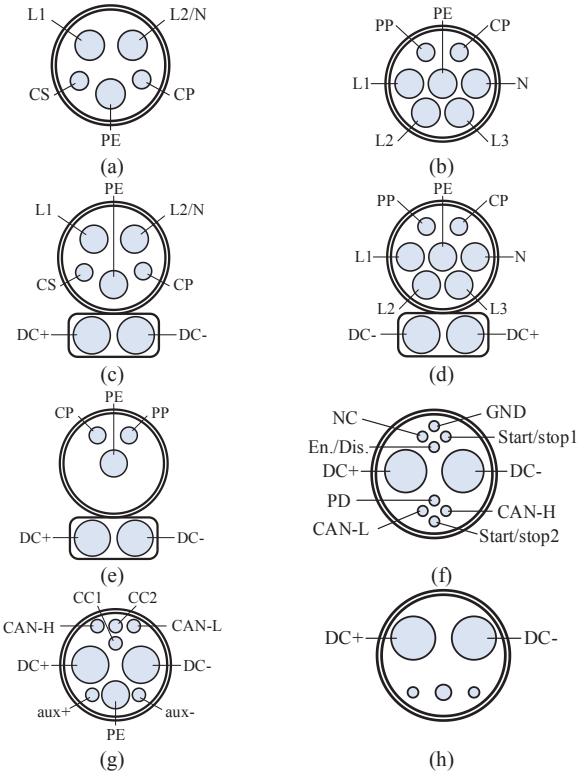

Fig. 2. Global male plugs [41]: (a) SAE J1772 (b) IEC 62196-2 Type 2 (c) CCS/Combo (US/Japan) (d) CCS/Combo (Eur.) (e) CCS/Combo (DC) (f) CHAdeMO[39] (g) GB/T 20234-3 (h) Tesla Supercharger.

TABLE II
GLOBAL EV POWER LEVEL CLASSIFICATION AND PLUG TYPES

SAE J1772 Level	Power Rating [kW]	Plug Type		
		US	Europe	China
AC Level-1	3.7	SAE J1772 Type 1	n/a	n/a
AC Level-2	3.7–22	SAE J1772 Type 1	IEC62196-2 Type 2	GB/T20234 AC
	≤22	Tesla	n/a	n/a
AC Level-3	22–43.5	SAE J3068	IEC62196-2 Type 2	GB/T20234 AC
DC Level-3	≤200	CCS Combo1 (SAE J1772 / IEC62196-3)	CCS Combo2 (IEC62196-3)	GB/T20234 DC
		Tesla Supercharger		
		CHAdeMO (IEC62196-3 Type 4)		

TABLE III
GLOBAL EV CHARGE PLUG CLASSIFICATION [41]

Standard	Voltage [V]	Current [A]	Peak Power [kW]
SAE J1772 Type 1 [38]	1Φ 120	≤16	1.92
	1Φ 240	≤32	7.68
IEC 62196-2 Type 2 [39]	1Φ 230	≤32	7.36
	3Φ 400	≤32	12.8
GB/T 20234 AC [40]	1Φ 220	≤32	7.04
	3Φ 380	≤32	12.16
Tesla Supercharger [44]	480	≤300	140
GB/T 20234 DC [40]	750	≤250	187.5
CHAdeMO [39]	500	≤400	200
CCS Combo1 [38],[39]	600	≤125	75
CCS Combo2 [39]	1000	≤200	200

2) Bidirectional Chargers: The typical structure of a bidirectional charger is shown in Fig. 3(b). Bidirectional chargers enable power flow control from the grid to the vehicle (G2V), as well as V2H, external load (V2L), or most commonly back to the grid (V2G). Together, V2H, V2L, and V2G power flow control will be designated as (V2x). In bidirectional OBCs, active front-end PFC stage and active DC-DC secondary side are necessary. Although bidirectional chargers can facilitate a variety of beneficial functionalities, they come at the price of more circuit components, which increases the system cost and reliability burden, and could slightly impact the power density and weight of the OBC.

D. Trends

There are three main trends in EV development that are significant to identify.

1) Increased Battery Capacity: Due to increased demand regarding the capability and range of EVs, propulsion battery capacities were forced to increase [8]. For example, the Nissan Leaf in 2013 had a battery capacity of 24 kWh [7]. Now, the Nissan Leaf in 2018 has a battery capacity of 110 kWh, as seen in Table I, representing a near 5-times increase over 5 years. This trend is expected to continue throughout the lifetime of EVs, facilitated by falling battery prices and increasing Energy and power densities of batteries throughout the 2020s [3],[46].

2) Increased Battery Voltage: Increased capacity of the propulsion battery may also be accompanied by an increase in the propulsion battery voltage [8]. For instance, the Porsche Taycan is one of the first vehicles to upgrade to a fully 800 V battery and electronics system [47]. However, upgrading the EV's propulsion battery voltage requires OEMs to also increase the operating voltage of other associated components, such as the OBC, APM and motor drive inverter. While these components are well-established in the market at 400 V, the market requires maturity for 800 V systems.

3) Increased OBC Power Level: Early EVs as identified in [7] utilized level-2 chargers with a peak power level of around 3.8 kW. Now, current vehicles come equipped with a level-2 OBC with a power range between 6.6 kW and 11 kW. This is primarily due to the trend of increasing EV battery capacity, in order for users to maintain reasonably fast charging times. Moreover, even though the DC fast charging infrastructure is growing, considerable strides need to be taken in order to accommodate oncoming demand. This infrastructure update will take considerable time and cost, as utilities need to update distribution components and off-board chargers need to be purchased and installed. Hence, incorporating high-power OBCs is a cost-effective intermediate solution to enable convenient onboard charging and alleviate range anxiety among EV owners.

4) Autonomy: Autonomous vehicles are becoming more and more prevalent in today's society. With increased autonomy comes increased computational demand by the vehicle's central computing system. Therefore, it is expected that vehicle's auxiliary batteries will have an increased role in the

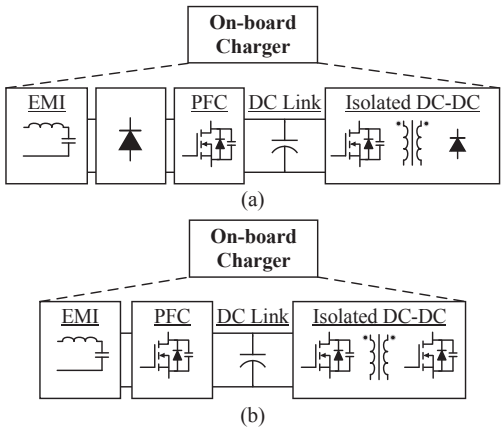

Fig. 3. Typical block diagram for (a) unidirectional and (b) bidirectional OBCs.

future of autonomous driving. Expectations include higher-rated APM, and perhaps increased auxiliary battery voltage to reduce cabling size, weight, and losses. With changes in the specifications of EV auxiliary batteries brings new challenges for the design and implementation of APMs.

E. Targets

The U.S. DRIVE Partnership is a collaboration between the Department of Energy (DOE), United States Council for Automotive Research (USCAR), five energy companies, and two utilities. In October of 2017, the U.S. DRIVE Partnership published a list of technical targets regarding various power electronics systems in EVs for 2020 and 2025 [48]. The targets included metrics of cost in ($/kW), specific power (kW/kg), power density (kW/L), and efficiency (%). The targets were posed for traction drive systems, power electronics, electric motors, DC-DC converters, and OBCs. In particular, targets regarding DC-DC converters (APMs) and OBCs are relevant for discussion. Based on current technology and research into DC-DC converters and OBCs, the targets are aggressive. Substantial research progress over the next three years will be required to meet the 2020 targets. The targets are summarized in Table IV.

TABLE IV
U.S. DRIVE 2020 AND 2025 TARGETS FOR DC-DC CONVERTERS AND OBCS IN EV APPLICATIONS [48].

Technical Component	Target Year	Cost [$/kW]	Specific Power [kW/kg]	Power Density [kW/L]	Efficiency [%]
DC-DC Converters	2020	<50	>1.2	>3.0	>94%
	2025	30	4	4.6	98%
OBCs	2020	50	3	3.5	97%
	2025	35	4	4.6	98%

III. ELECTRIC VEHICLE OBC TOPOLOGIES

Due to the identified trends in EVs regarding increased battery capacity and hence increased OBC power rating, OBC converter topologies strictly greater than 7.4 kW will be identified and analyzed in this section, coming from both industry as well as research environments.

A. Industry Established Charging Solutions

Currently, at least four Tier 1 suppliers offer high-power OBC solutions that can be designated as the industry state-of-the-art. The following information was found using available primary online resources, and thus this list may be incomplete, as many companies and EV manufacturers do not release their OBC information because of competitive privacy reasons.

1) Brusa [49]-[51]: Brusa offers the NLG664 and NLG667 on-board chargers, which are both liquid-cooled and compatible with up to 7 kW single-phase and 22 kW three-phase. They achieve three-phase efficiency of over 94% and single-phase efficiency of over 90%, with 1.83 kW/kg specific power, and 1.82 kW/L power density. Finally, according to [59], the chargers utilize conventional Si switching devices.

2) G-Power [52]: The G-Power OBC can operate as either a 10 kW three-phase charger, or a 6.6 kW single-phase charger. The OBC achieves 94% efficiency, and a 0.52 kW/L power density. Furthermore, the charger is air-cooled, which is likely the main contributor to its large volume.

3) Continental [53]: The Continental OBC is a single- and three-phase compatible charger supporting power levels up to 22 kW. A detailed datasheet including figures for peak converter efficiency, power density, and weight is not available at this time.

4) Delta [54]: Delta offers an on-board EV charger that is compatible with up to 10 kW input power. While technical specifications are not detailed online, [54] provides a detailed thermal analysis for the liquid cooled thermal management of the OBC. The topology is shown to be a totem pole bridgeless boost PFC, isolated LLC resonant converter, and output rectification with a diode bridge. The charger achieves a maximum efficiency of 95.8%, and a 1.4 kW/L power density with Si devices or a 2.5 kW/L power density with GaN devices. It should be noted that the GaN version is intended solely for research purposes, due to current high cost of GaN switches and non-availability of sufficient reliability data.

5) Discussion: Each of these industry-level chargers are capable of operating over a wide input voltage range and variable grid frequency. The benefit of the wide input voltage and grid frequency ranges is that the charge is compatible with the global EV market and EVSE units. Furthermore, each charger is capable of a wide output voltage range variation in order to charge the EV's propulsion battery throughout the full state-of-charge profile. For instance, an EV's typical 400 V propulsion battery pack could have a terminal voltage around 250 V at low state-of-charge. Finally, in terms of efficiency, power density, and specific power, none of the presented commercially available OBCs meet the U.S. Drive Partnership's 2020 targets, illustrating the need for increased research and development.

The information from this section is summarized in Table IV. OBC research and development should seek to satisfy similar input and output specifications, while aiming to meet and exceed the cost, efficiency, power density, and specific power metrics, per the U.S. DRIVE Partnership targets. While it is believed that other companies, including but not limited to Tesla and Shinry Technology, also offer high-power OBC

solutions, their product specifications are not detailed in available primary sources.

B. Non-integrated OBCs

Several non-integrated high-power OBC topologies and their associated control algorithms have been researched in the literature. As previously defined, a non-integrated OBC is a unique component inside the EV that interfaces the charging input and provides conditioned output power to the high-voltage propulsion battery. The typical structure of a non-integrated OBC includes an electromagnetic interference (EMI) filter, an AC-DC PFC, a DC link, and an isolated DC-DC converter. One of the primary difficulties in high-power OBCs is balancing efficiency, cost, size, reliability and weight. Efficiency and cost considerations are particularly important at higher power levels because the current-related conduction losses may be high, and thus paralleled switching devices may be required. The presented strategies each approach this issue in different ways. While most of these topologies are two-stage, several single-stage topologies are also identified. Single-stage topologies may be advantageous to meet stringent power density requirements posed by auto manufacturers and the U.S. Drive Partnership targets, in addition to saving weight, reducing cost, and enhancing reliability with the removal of the electrolytic DC link capacitor [55]. This section provides a review of all high-power (>7.4 kW) non-integrated OBCs available in the literature, to the best knowledge of the authors at the time of authorship.

1) Modular Two-stage Solution 1 [56]: The circuit topology of a single-phase module of this three-phase charger can be seen in Fig. 4(a). While this converter is rated for 10.5 kW, it utilizes three parallel single-phase charging modules each rated for an equal distribution of full power, at 3.5 kW. Each single-phase charger is composed of a diode bridge and a boost converter operating at 90 kHz switching frequency, connected to a DC link. The DC-DC stage for each single-phase unit is an isolated half-bridge LLC resonant converter, with a diode bridge at the secondary side. The half-bridge LLC converter is operated using frequency modulation with a switching frequency range between 90 kHz-275 kHz. There is a single input filter with a high EMI filtering requirement from each of the three single-phase converters. While the burden on the input and output filters is high, there are no duplicate filtering elements in the circuit as compared to having filters for each phase.

The PFC and LLC stages are independently controlled by respective digital signal processors (DSPs), which communicate with one another over a serial communications interface (SCI). Each PFC DSP is responsible for conditioning the input current, ensuring near-unity power factor, and charging the DC link capacitor to the requested voltage from the LLC DSP. On the other hand, the LLC DSP is responsible for regulating the DC-DC stage switching frequency to achieve the desired output voltage and current requested by the vehicle BMS.

TABLE V
COMPARISON OF COMMERCIALLY AVAILABLE OBCS

OBC		V_{in} [V]	V_{out} [V_{DC}]	Rated Power [kW]	η [%]	Power Density [kW/L]	Specific Power [kW/kg]
[50]	1Φ	200-250	200-450	7	>90	1.82	1.83
	3Φ	360-440	310-430	22	>94		
[51]	1Φ	200-250	360-750	7	>90	1.82	1.83
	3Φ	360-440	570-750	22	>94		
[52]	1Φ	176-264	250-420	6.6	>94	0.52	-
	3Φ	304-456		10			
[53]	1Φ	120-240	220-470	7	-	-	-
	3Φ	208-416	450-835	22			
[54]	1Φ	85-264	200-400	10	95.8	1.4 Si 2.5GaN	-

It is reported that the converter achieves an efficiency of 95.6%, and a power density of 1.75 kW/L. An advantage of this design is modular power processing, zero-voltage switching (ZVS) capabilities in the half-bridge LLC switches, and reduced system complexity with the PFC input and LLC secondary side diode bridges. Disadvantages include unidirectional power flow, additional system weight and size in the output filter inductor, and reliability concerns in the use of the DC link and high-stress on resonant capacitors.

2) Modular Two-stage Solution 2 [57]: The circuit topology of a single-phase module of this three-phase converter is shown in Fig. 4(b). The modular 3-phase charger is rated for 22 kW for the European grid, and 17.2 kW for the US and Japanese grids. Similar to [56], there are three modular units, each of which ideally processes one third of the rated power at 7.4 kW in Europe, and 5.73 kW in the US or Japan. Each single-phase unit is comprised of a diode bridge with an inrush current limiter, and an interleaved boost converter connected to a DC link. The inrush current limiter is significant to facilitate the start-up performance of the OBC. The DC-DC stage of each single-phase unit is two parallel input, parallel output isolated full-bridge LLC resonant converters with diode bridges at the secondary side.

The interleaved boost converter is responsible for shaping the input current, and also variable DC link voltage control to maximize the efficiency of the parallel full-bridge LLC converters. Interleaved boost converters reduce the required inductance of the boost inductors by half, which can improve the power density of this stage [1]. Furthermore, the EMI input filter requirement is reduced because the interleaved boost converter input current ripples are 180° out of phase [58]. The parallel LLC converters operate using a constant switching frequency and phase-shift control technique, which controls a variable phase-shift between switches S_{3x} and S_{6x}, and complimentarily S_{4x} and S_{5x}, for x = (a, b). One of the main problems in parallel LLC converters is unequal current sharing and different gain characteristics due to uncontrollable component tolerances in the two resonant tanks. Therefore, the primary reason for utilizing the phase-shift control in this case was to eliminate the possibility of different switching frequencies in the two LLC converters, which can lead to beat frequency problems in the system. Beat frequency effects

could generate critical low frequency input and output current ripples, which would require substantial filtering efforts. It is reported that the converter achieves a peak efficiency of 94.5%, a power density of 1.98 kW/L, and a weight of 12 kg.

Advantages of this design include reduced current ripple in the output capacitors with interleaved phase shift control, and compact charger size. Disadvantages include unidirectional power flow, and a large number of circuit components although only ten are active switching devices per phase.

3) Modular Single-stage Solution 1 [59]: The circuit topology of a single-phase module of this three-phase converter can be seen in Fig. 4(c). This charger is designed for 22 kW and is composed of three single-phase 7.2 kW units. Each single-phase unit is comprised of a full-bridge switch network R_1-R_4, which is operated as a full-wave rectifier. This leads to a rectified AC voltage across the AC link capacitor bank, C_{AC}. Since the AC link capacitor is not an energy storage capacitor, the topology is designated a single-stage solution. Following the AC link in each single-phase unit is an isolated full-bridge dual-active-bridge (DAB) DC-DC converter. Four GS66516T devices are utilized in parallel to enhance the thermal performance of the charger, and proper current sharing is achieved and examined.

With the front-end full-bridge only offering rectification, the DAB converter is therefore responsible for shaping the input current to achieve PFC action. In this case, a secondary side dual-phase-shift (SDPS) control strategy is developed, which can shape the input current accurately as well as offer ZVS on every switch. The two control variables are the phase shifts for each of the two secondary side bridge legs (S_1, $\overline{S_2}$) and (S_3, $\overline{S_4}$) referenced to the primary side bridge leg (P_1, $\overline{P_2}$), while the bridge leg (P_3, $\overline{P_4}$) is 180 degree phase shift from (P_1, $\overline{P_2}$). When the battery voltage is low, a primary-side dual-phase-shift (PDPS) control strategy is utilized to ensure ZVS operation and reduce DC-DC converter MOSFET current stress. The two control variables are the phase shifts for the primary side bridge leg (P_3, $\overline{P_4}$) and secondary bridge leg (S_1, $\overline{S_2}$) referenced to the primary side bridge leg (P_1, $\overline{P_2}$), while the bridge leg (S_3, $\overline{S_4}$) is 180 degree phase shift from (S_1, $\overline{S_2}$). Finally, a third control strategy utilizing a triple phase-shift (TPS) is developed to enhance the light load performance of the converter. The control variables are the phase shifts of three bridge legs (P_3, $\overline{P_4}$), (S_1, $\overline{S_2}$), and (S_3, $\overline{S_4}$) with reference to the primary bridge leg (P_1, $\overline{P_2}$). In every mode, the duty cycle for each bridge leg switch is 50%.

In comparison to [60], where a direct matrix converter is used to directly convert single-phase AC to DC, the topologies of the two converters are similar. The downside of the structure in [60] is the necessity of bidirectional switches to accommodate the positive and negative half cycles of the input voltage. This doubles the switch and driving circuit count where expensive GaN devices are required in parallel for thermal and loss considerations. For the case shown in Fig. 4(c), since the front-end rectifying bridge switches at mains frequency, conventional Si MOSFETs are suitable because the

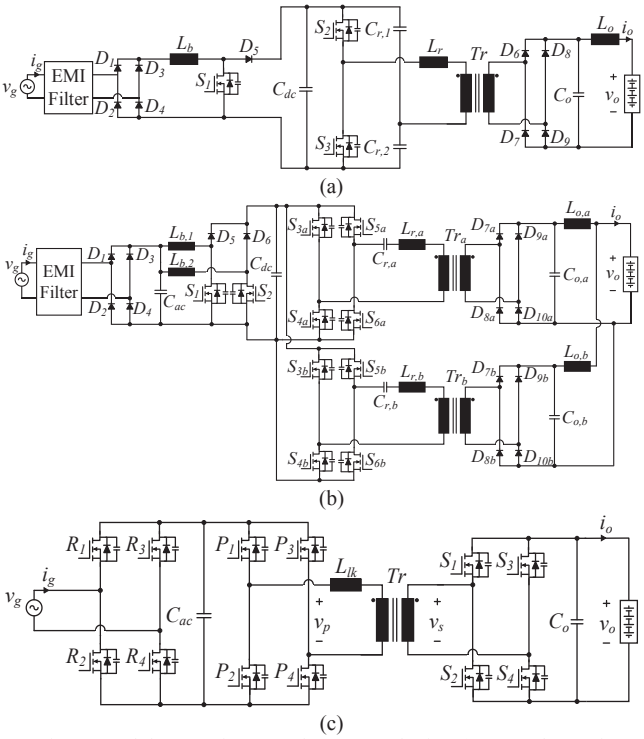

Fig. 4. Modular, non-integrated OBC topologies: (a) One phase of topology [56]; (b) One phase of topology [57]; (c) One phase of topology [59].

only important switch characteristic is the on-state resistance. Furthermore, an additional advantage of the rectifying bridge in Fig. 4(c) is the reduced RMS current than the back-to-back switch network in [60]. One area of concern in the proposed charging system is the high source and sink characteristics of the AC link, however this AC link capacitor bank can be realized with much smaller form factor than its DC link counterpart.

The 22 kW charger utilizes GaN devices and achieves both a high power-density and high efficiency. A direct comparison is made to the Brusa NLG664, and efficiency improvements after around 7 kW input power are demonstrated. Additionally, the authors constructed a SiC prototype and drew comparisons between the two emerging wide bandgap (WBG) technologies in [61]. It was concluded that the GaN prototype exceeded its SiC counterpart in the categories of efficiency, power density, and projected 2020 cost.

It is reported that the charger achieves peak efficiency over 97%, and a power density of 3.3 kW/L. Advantages of this design include no DC link capacitor, very high power density, and high converter efficiency. Disadvantages of the charging system include the addition of active components for single-phase implementation, high cost of GaN components at the current price levels, and a complex control implementation.

4) Full-power Two-stage Solution 1 [62]: The circuit topology of this converter can be seen in Fig. 5(a). The charger is designed for 10 kW power rating utilizing a three-phase input connection. The charging unit is comprised of a three-phase boost PFC connected to a DC link capacitor, followed by an isolated LLC resonant DC-DC converter with half-bridge structure at the primary side, and a full-bridge

topology on the secondary side. The charging unit also has an additional input connection to the DC link from a boost converter that connects to a solar panel input, which was omitted from the circuit schematic for compactness.

While the authors do not mention the control technique for the three-phase boost PFC, several related documents regarding control with a single DC link voltage sensor, duty cycle compensation, and a soft-switching strategy can be found in [63]-[65], respectively. On the other hand, the half-bridge LLC resonant converter is controlled using typical frequency modulation, with the switching frequency varying between 90 kHz-150 kHz. One desirable control capability of the front-end PFC is variable DC link voltage control to maximize the efficiency of the cascaded DC-DC converter.

It is reported that the converter achieves an efficiency of 96%; however, numbers for power density and weight were not provided. An advantage of this design is reduced system complexity for high-power compatibility, bidirectional power flow due to the active front end and DC-DC secondary sides, and comparatively high efficiency. However, disadvantages lie in the high RMS currents of the half-bridge LLC, reliability due to higher stress on resonant capacitors, and high EMI filter requirement due to the active front-end PFC.

5) Full-power Two-stage Solution 2 [66]: The circuit topology of this converter is shown in Fig. 5(b). The charger is designed for 20 kW power rating with a three-phase input. It is comprised of a three-phase boost PFC connected to a DC link capacitor, followed by two parallel connected isolated half-bridge LLC resonant DC-DC converters, with two high frequency transformers (HFT) connected in series-star configuration, and two parallel secondary side diode bridges. The two HFTs, connected in series-star configuration, are significant to ensure equal current flow between the primary sides of the two DC-DC converters, mitigating resonant component discrepancies between the two converters. By utilizing a relay on the star point, between nodes R_1 and R_2 in Fig. 5(b), the circuit could be reconfigured to operate without the second DC-DC converter unit in lower power modes.

The PFC and DC-DC converters are independently controlled by respective DSPs. The three-phase boost PFC is controlled with discontinuous pulse width modulation (DPWM) in combination with a direct-quadrature (DQ) reference frame current loop and an outer DC bus voltage loop, both supplied with reference signals by a phase-lock loop (PLL). The DPWM control strategy is utilized over the traditional space vector pulse width modulation (SVPWM) technique in order to achieve a higher DC link voltage of over 600 V and reduce switching loss, at the cost of increased conduction loss. Additionally, variable DC link voltage control is utilized to achieve maximum efficiency through the isolated DC-DC converters. On the other hand, the half-bridge LLC utilizes traditional frequency modulation to fulfill the output voltage and current requests from the vehicle's BMS. A 180-degree phase shift is incorporated between the two primary side half-bridges to simplify the current loop control

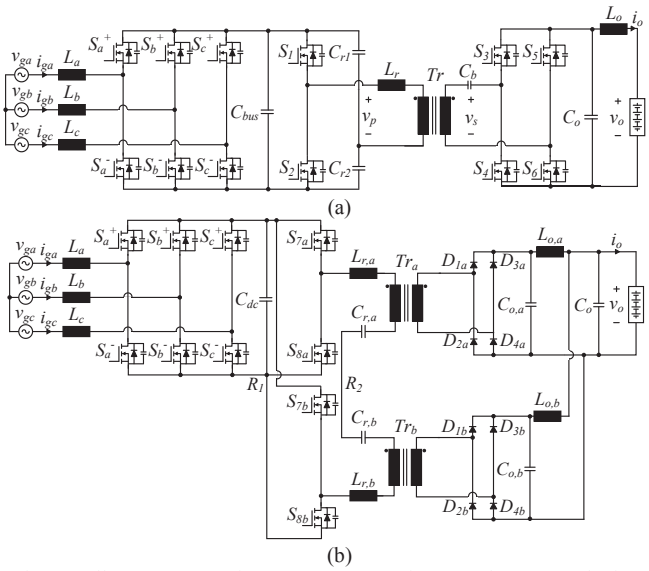

Fig. 5. Full-power processing, two-stage, non-integrated OBC topologies: (a) Topology [62]; (b) Topology [66].

to a single PI loop. Finally, the secondary side diode bridges can be reconfigured from a parallel to series connection to realize an output voltage range from 400 V_{DC} to 900 V_{DC}.

One important consideration that is neglected in this study is the size, weight, volume, and efficiency contributions from the input EMI filter. Comprehensive design approaches and optimization for both common-mode (CM) and differential mode (DM) filters in the three-phase boost PFC have been systematically evaluated in [67],[68]. The EMI filter is particularly significant in the three-phase boost PFC as there is an inherent requirement for attenuation of high frequency CM components [67]. Additionally, DM filter optimization can lead to a compact and lightweight contribution of the filter to the overall system, which is addressed in [67] and [68].

It is reported that the converter achieves an efficiency of 96%; however, power density and weight numbers were not provided. Advantages of the converter include flexible output voltage range capabilities, accurate current sharing with star connection between the two transformers, and high-power processing at a reasonably high efficiency (although the efficiency measurements are not given the authors mention a peak larger than 96%). Disadvantages include potentially high RMS currents at 20 kW through the half-bridge LLC primary side, reliability concerns in the DC link and resonant capacitors, and unidirectional power flow due to use of secondary side diode bridges. Bidirectionality could be achieved using secondary side full-bridge MOSFETs at the cost of increased system complexity.

6) Full-power Processing Single-stage Solution 1 [69],[70]: The circuit topology of this converter can be seen in Fig. 6(a). The charger is designed for a 10 kW power rating utilizing a three-phase input connection. The charger is realized using a 3-phase matrix converter with back-to-back switches, a link inductor, an HFT, and a full-bridge active secondary side. The HFT and additional link inductor, *L*, are designed and optimized for high efficiency and low volume in [71]. Due to

the single-stage nature of this system, PFC input inductors and the DC link capacitor are removed; however, the number of switches and driving component stress increases due to the necessity of primary side back-to-back switches, as demonstrated in [72]. This design is shown to achieve a more compact and lightweight solution compared to the three-phase voltage source converter and a full-bridge DAB [72].

Since the matrix converter is voltage fed, only one input phase can be connected to either the positive (P) or negative (N) transformer terminals at any time. However, the transformer current must remain continuous at all points in time due to its inductive nature. Therefore, a switching space vector combined with phase shift modulation is utilized as the control strategy [73]. A reactive power component is also present and should be compensated in order to realize high converter efficiency. An additional control strategy utilizing optimal reactive power minimization can be found in [74].

It is reported that the power density of the functional prototype is 0.67 kW/L with a specific power of 0.84 kW/kg, however this prototype was merely utilized to validate the technology. A full enclosure design has not yet been designed and optimized but it is expected that a significant increase in the power density and reduction in weight could be achieved. Advantages of this converter include single stage nature and thus high potential power density, bidirectional power flow capability, and reactive power compensation to the 3-phase input. Disadvantages of this converter include complex control implementation, challenging compatibility with single-phase input due to output power pulsation at double mains frequency, and a high semiconductor count due to the necessity of bidirectional switches on the primary side.

7) Full-power Processing Single-stage Solution 2 [75]: The circuit topology of this converter can be seen in Fig. 6(b). The charger is designed for 11 kW power rating utilizing a three-phase input connection. The charger is realized using three AC ports with T-type circuits, a three-port HFT, and an active full-bridge secondary side. The T-type circuits connect the three-phase AC system to each of the three transformer ports and a virtual star point. The HFT consists of four windings, three for the AC-side and one for the DC-side, and the leakage inductance acts as the energy transfer element, saving one additional magnetic circuit component.

The T-type multi-port charger is operated using phase-shift control, similar to a DAB. ZVS is achievable for all switches over the whole AC line period using the novel approach presented in the included reference. It is reported that the converter achieves a 96% efficiency and a power density of 2.5 kW/L. Advantages of the converter include a compact design, small allowable value of the output capacitor due to ripple cancellation, and bidirectional power flow capability. Disadvantages include a high primary side semiconductor count, difficult single-phase implementation, and a complex control scheme.

8) Discussion: In order to reduce the current stress in the primary side bridge of [56], [62], and [66] which use half-

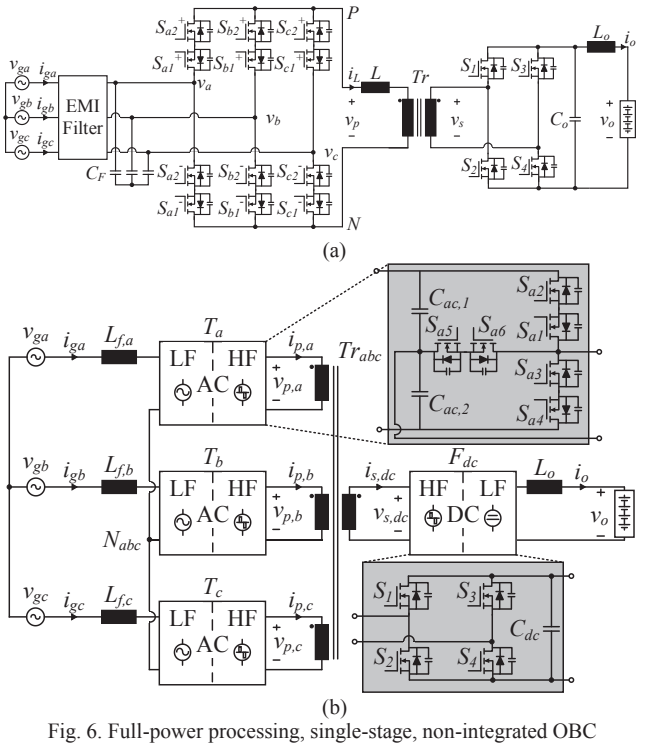

Fig. 6. Full-power processing, single-stage, non-integrated OBC topologies: (a) Topology [70]; (b) Topology [75].

bridge LLC resonant DC-DC converters, the full-bridge LLC resonant DC-DC converter is a viable solution. While reducing the high primary side RMS currents, the addition of two switches introduces more circuit components in the addition of two switches and associated driving components, and thus slightly increases circuit cost and charger size. However, with an appropriate control algorithm these switches can also achieve ZVS turn-on and would only be subject to turn-off and conduction losses. The comparison between these two topologies at 1 kW can be seen in [76], and specific device-related stresses of the half-bridge LLC converter are shown in [77]. Although the half-bridge converter is preferred up to 1 kW, it is expected that increases in the power level will eventually see efficiency benefits in the full-bridge converter due to the reduced RMS current.

Aside from [59] and [75], all of the designs utilize a transformer and additional resonant inductor, as opposed to an integrated transformer that realizes the resonant inductance through the leakage inductance. Magnetic design integration can eliminate an additional bulky magnetic component, leading to a more compact and lightweight charger design. A novel winding strategy for planar transformers to create variable leakage inductance, while minimizing the winding's AC resistance, has been recently proposed in [78].

The two modular three-phase unidirectional solutions presented in Figs. 4(a) and 4(b) could be converted into bidirectional units with the addition of an active front-end PFC, for example the interleaved totem pole PFC or H-bridge boost PFC. Furthermore, the secondary side diode bridges would need to be replaced by active semiconductor devices. The utilization of an active secondary side would also lead to efficiency improvement of any resonant-based topology, for

example the DC-DC stage of the topologies in Figs. 5(a) and 6(b). Switches are advantageous over diodes because they have a smaller total conduction loss. The switches should be controlled by synchronous rectification (SR), to minimize hard-switching loss by turning on the devices at the zero crossing of secondary-side current. In order to accurately implement SR, knowledge of the secondary-side current's phase is required. A study in [79] has shown that SR implementation cannot be guaranteed by the first-harmonic approximation (FHA), especially away from resonant frequency operation, and thus an extended-harmonic analysis (EHA) model is required and synthesized. Implementation of the EHA secondary-side SR control is shown to increase the efficiency of a CLLC converter at 1 kW by 6.8% and 1.8% over the utilization of a diode full-bridge and FHA-based SR control, respectively.

The chargers in Figs. 4(a), 4(b), and 4(c) are compatible with single-phase input connections without any main-circuit reconfiguration. However, due to the single-stage nature of the topology in Fig. 4(c), an additional active filter circuit is required in single-phase operation to remove the double mains frequency component from the output power.

The three-phase boost PFCs utilized by the two-stage full-power processing converters presented in Figs. 5(a) and 5(b) can also be operated with single-phase input connection. To enable this mode of operation requires disabling one switching leg, for instance S_c^+ and S_c^-, and connecting the line terminal of the single-phase input to the A-phase and the neutral terminal to the B-phase. The A- and B-phase bridge legs can then be operated as a typical H-bridge PFC. A duty compensated reduced harmonic control for the single-phase H-bridge PFC can be found in [80]. Furthermore, the current waveform generated by the H-bridge PFC can be further improved achieving higher conversion efficiency, and reduced peak to peak ripple according to a recent study carried out between PI and Type-II compensators [81]. From another perspective, the three-phase boost PFC can be operated in single-phase as a bridgeless totem-pole interleaved boost PFC, by connecting the line terminal of the single-phase input to the A- and B-phase and the neutral terminal to the C-phase. The equivalent circuit is identical to the traditional bridgeless totem-pole interleaved boost PFC circuit with equivalent inductances larger than L_x (x = a, b, c). The topology can be controlled using a dual closed-loop PI-based technique exhibited in [82], however the input current will have zero-crossing distortions. To improve the system dynamics and significantly reduce zero-crossing input current distortions, the topology can be controlled with a sliding mode approach proposed in [83].

It is evident that the single-stage charger in [59] and shown in Fig. 4(c), utilizing an AC link capacitor and GaN devices, achieves the highest power density and efficiency. It is believed that an optimized prototype of the three-phase matrix converter in [70] and shown in Fig. 6(a) may achieve comparable power density. The T-type converter also exhibits high power density. Therefore, single-stage solutions appear preferable over two-stage solutions in terms of power density. However, it is significant to note that none of the presented high-power OBC structures currently meet the U.S. Drive Partnership 2020 power density target of 3.5 kW/L, demonstrating the need for additional research in OBC miniaturization.

The key characteristics of non-integrated high-power OBC solutions presented in this section are summarized in Table V.

C. Additional AC-DC Converter Considerations

1) Swiss Converter: A high-power OBC system typically utilizes an AC-DC PFC stage with a single DC link capacitor bank, followed by either a DC-DC converter, or two DC-DC converters in parallel. However, the Swiss front-end, presented in [84], is an active AC-DC front-end topology that sets up parallel DC-DC converter connections inherently, which makes it an interesting candidate for high power OBC systems. The circuit topology of the Swiss is presented in Fig. 7(a). This topology is advantageous due to mains frequency commutation of the MOSFETs, and hence negligible switching losses. In [84], an 8 kW non-isolated rectifier resulted in only 15.4 W of total loss. Furthermore, as previously mentioned, the topology sets up the use of two series input, parallel output isolated DC-DC converters. However, these DC-DC converters need to be able to shape their input current to a DC offset rectified sinusoid in three-phase conduction, or a rectified sinusoid in single-phase connection. In single-phase connection, a relay could be utilized to open the S^-/R^- node, and reconnect R^- to R^+, such that the two DC-DC converters would be parallel connected on both the input and output. Therefore, the Swiss front-end combined with two parallel DC-DC converters could potentially result in a compact, lightweight, and high efficiency OBC solution.

2) Modular multi-level converters (MMC): In the past, the MMC topology for AC-DC power conversion shown in Fig. 7(b) has been primarily utilized for high-voltage (hundreds of kVs) and high-power (hundreds of kWs) applications. However, a recent study in [85] has investigated the topology's use as a front-end AC-DC PFC stage in a 6.6 kW OBC. The authors mention that the applicability of MMCs to OBC systems has become practical with the emergence of reliable, low-voltage GaN devices with higher $R_{ds}Q_g$ figure-of-merit (FoM) than high-voltage Si or SiC devices. The study in [85] compares a 6.6 kW two-level AC-DC PFC topology to a six-level (n = 6) MMC over power quality, EMI considerations, loss breakdown, and volume.

The results in [85] demonstrate that the MMC could potentially be advantageous over the compared two-level topology in terms of total passive component volume, efficiency, and active component footprint area. It is mentioned that the MMC requires a large capacitance C_{sm} in each module but no DC link capacitance, because the C_{sm} capacitors collectively behave as a DC link capacitor with net capacitance $C_{dc} = 2C_{sm}/N$. In terms of efficiency, the authors

TABLE VI
NON-INTEGRATED OBC COMPARISON

Topology	Power Rating [kW]	Efficiency	Power Density [kW/L]	Specific Power [kW/kg]	Bidirectional Operation?	DC Link?	# Inductors	# Switches	# Diodes	# Transformers	# Capacitors
[56]	10.5	95.6%	1.75	-	N	Y	7	9	27	3	12
[57]	22	94.5%	1.98	1.83	N	Y	18	30	42	6	18
[59]	22	>97%	3.3	-	Y	N	3	36	0	3	6
[62]	10	96%	-	-	Y	Y	5	12	0	1	5
[66]	20	96%	-	-	N	Y	7	10	8	2	6
[70]	10	-	0.67	0.84	Y	N	2	16	0	1	4
[75]	11	96%	2.5	-	Y	N	4	22	0	3	7

"-" Denotes that the metric was not provided in the reference.

present 96.31% efficiency for the two-level topology compared to 98.22% for the MMC, at 5 kW. However, one metric that was not addressed in this manuscript is a cost comparison. The cost of a six-level MMC would be much higher due to the very high switch count (48 active devices) and current cost of GaN devices. Additionally, while the MMC exhibits lower active device conduction and switching losses, the thermal design may be challenging due to the high device count.

D. Additional DC-DC Converter Considerations

One of the challenges in high-power OBCs is an effective distribution of the charging current in the isolated DC-DC converter stage to minimize the conduction loss in the switches and transformer windings. The three-phase CLLC proposed in [86] is a newly developed isolated DC-DC converter candidate that could be beneficial in high-power applications. The circuit topology of this converter is presented in Fig. 7(c). This three-phase CLLC DC-DC converter is designed for 12.5 kW power rating utilizing three CLLC converters in delta connection on the primary side, a three-phase HFT, and parallel connected full-bridge rectifiers on the secondary side. The primary side delta connection does not have difficult start-up conditions, as does its Y-connected counterpart; furthermore, it ensures equal current sharing through each of the three resonant tanks. High frequency switching at 500 kHz facilitates the use of planar magnetic transformers, which is a key enabler in achieving high power density. Furthermore, the planar transformer is realized as a matrix transformer, with delta connected primary windings and parallel connected secondary windings. Therefore, each secondary side converter ideally processes only 1/3rd of the full power of the converter, helping to minimize conduction loss in the secondary-side windings and MOSFETs.

While the primary contribution from [86] is the integrated and optimized transformer design, the experimental results demonstrate the potential for the delta-connected three-phase CLLC converter in EV OBC applications. The circuit achieves a 9.46 kW/L power density with a peak efficiency over 97%, and over 96% efficiency for 2/3rd of the operating range.

On another note, [86] provides a brief review of the turn-on and turn-off characteristics of three different SiC MOSFETs rated for over 1 kV and 19.7 A: C2M0025120D, C3M0065100K, and C3M0075120K. In conclusion, it is shown that the Gen. 3 SiC devices with four-lead packages perform significantly better in terms of turn-on and turn-off speed as well as reduced gate signal ringing, compared to the conventional Gen. 2 three-lead package. Analysis of switching characteristics is a necessity for proper selection of semiconductor devices for any high-power applications.

E. Propulsion System Integrated OBCs

A presentation on the current state-of-the-art in EV OBCs would be incomplete without a review of research into high-power integrated OBCs. Integrated OBCs designate that on-board charging functionality is combined with other existing and necessary components within the EV. The most popular integration companion for high-power EV OBCs is the propulsion system, consisting of the electric motor and motor drive inverter. The combination of the EV motor and drive inverter include all of the necessary components in a typical OBC system (switch, diode, inductor, and capacitor). Therefore, with the addition of a front-end grid-to-motor interface or possible reconfiguration of the motor windings, high-power charging can be accomplished without generating a torque in the motor. The block diagram of a typical propulsion system integrated OBC is shown in Fig. 8(a). From Table I it is evident that typical EV motors are rated between 30 kW and 200 kW, which establishes the possibility of propulsion integrated on-board chargers to compete with off-board fast DC charging systems. One downside of propulsion machine integration however might be increased stress on the propulsion system. The Renault ZOE currently utilizes a propulsion machine integrated OBC called the Chameleon charger, patent protected in [87] and [88], accepting 3 kW-43 kW power levels through the propulsion machine [14]. Additionally, the Continental AllCharge, set for release in 2022, employs a bidirectional propulsion machine integrated OBC structure that only adds a DC-DC converter to the electrical system, and supports power levels up to 43 kW [42].

Propulsion system integrated OBCs can be broadly organized into five categories based on interfacing requirements: access to the motor's neutral point [87],[88], split motor windings [89],[90], reconfiguration of motor windings [91], multi-phase propulsion system [92]-[94], and add-on interface systems [95],[96]. As a brief background,

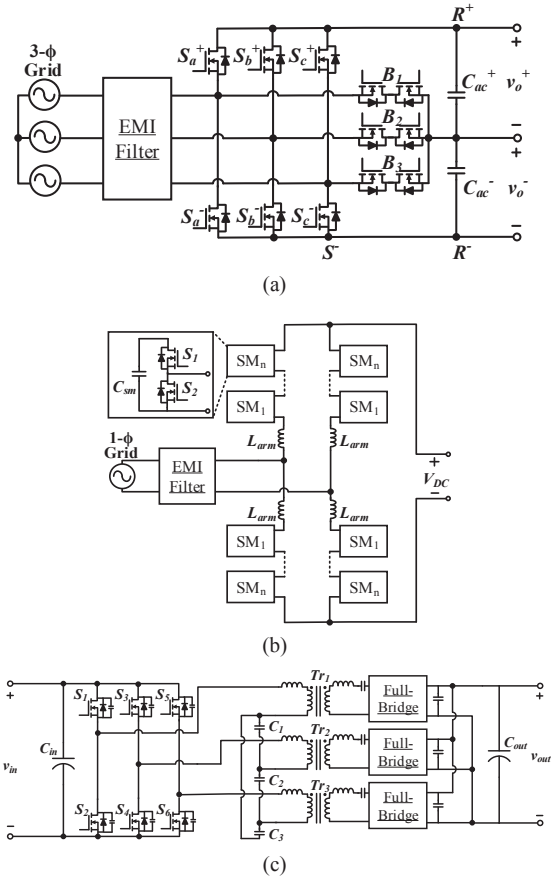

Fig. 7. Additional converter considerations: (a) Swiss front-end (b) Modular multi-level converter (c) Three-phase CLLC.

many different structures for propulsion integrated OBCs have been proposed; however, most require a modified propulsion system or a custom designed electric machine to be suitable for the charging mode of operation. In particular, the Chameleon charger from Renault utilizes the access to the motor's neutral point to reconfigure the motor inverter into three individual boost converters. Much of the work on propulsion integrated OBCs has previously been reviewed in [7], however two recent additions are presented here.

1) Multi-phase Propulsion System: A multi-phase propulsion system integrated charging technique was developed as a means of eliminating the need for any additional on-board components to facilitate battery charging, while avoiding torque generation in the propulsion system during charging. In this multi-phase propulsion integrated OBC method, the propulsion machine inductors are decoupled and utilized as the input filter inductors to the multi-phase inverter acting as a three-phase AC-DC converter directly connected to the vehicle's propulsion battery. Integrated charging has been demonstrated on propulsion systems consisting of an asymmetrical nine-phase machine [92], an asymmetrical six-phase machine [93], and a five-phase machine [94]. Since the inductance decoupling is similar for each type of machine, a circuit topology for the five-phase machine is presented in Fig. 8(b) for compactness. While [92]-[94] describe the charging methods for three-phase input excitation, [97] develops single-phase charging provisions for all three types of machines. Furthermore, bidirectional power flow capability is demonstrated in each case.

A full overview of multi-phase propulsion system integrated OBCs and their control algorithms can be found in [98]. The primary disadvantage for multi-phase propulsion integrated OBC systems is that three-phase propulsion machines currently dominate EV propulsion systems, and thus this charging technique may have limited implementation capabilities [95].

2) Add-on Interface [95],[96]: The implementation of a propulsion machine integrated OBC would be a promising solution if it does not require any modifications to the typical three-phase propulsion system. In [95] and [96] neither modification is made to the motor, nor special propulsion system designs are required. The charging system simply requires an additional buck-type three-phase full-bridge unit and an EMI filter to interface the connection between the three-phase grid and the motor. The full topology of the charging system can be seen in Fig. 8(c). In this configuration, the EMI stage, switches S_1-S_6, and diodes D_1-D_6 are within the add-on interface, and the propulsion machine is decoupled to realize three distinct inductors during the charging mode of operation. Although this additional interface unit is required, it can be designed to be very compact, as it requires only six switches and associated gating modules, six diodes, and an EMI filter. Control for the three-phase input mode of operation can be found in [99]. Additionally, single-phase operation and control of this charger can be found in [100]-[101]. Bidirectional power flow is also possible with this charging architecture, however the control has yet to be developed. A similar approach to Fig. 8(c), which connects the add-on interface to the midpoint of the motor windings, was researched in [102]. However, the system is inhibited by resonance in the input filtering stage, requiring computationally expensive active damping (AD) control.

IV. Charging Infrastructure Considerations

A. Infrastructure-based Charging Strategies

Due to the year-over-year projected influx of EVs across the world, more intelligent charging of EVs will be necessary to realize EVs full benefits in the electric grid and protect potentially at-risk distribution systems. Case studies in Greece and Toronto have been carried out in [103] and [104], respectively. In Greece, large EV deployment resulted in voltage deviation violations in rural electric network lines, as well as overloading in urban electric network lines. However, smart, coordinated, charging methods were shown to alleviate these problems and enable higher EV penetration rates. In the case of Toronto, while slow EV OBCs (<6.6 kW) were not likely to cause significant overloading problems to the local electric grid, the long charging times were seen to absorb available spare capacity of transformers and negatively affect their cooling cycles. On the other hand, higher power OBCs (≥6.6 kW) showed significant impact on equipment capacity and margins of safe operation, and it was therefore

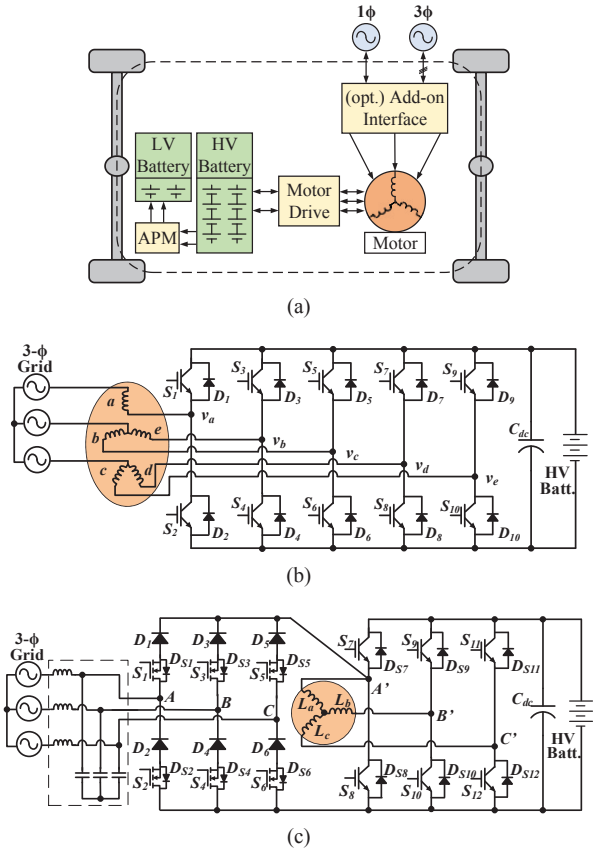

Fig. 8. Propulsion integrated OBC (a) block diagram (b) with multi-phase propulsion system [98] (c) with no modifications to propulsion system [95].

recommended for utilities to upgrade the electrical equipment before accommodating these chargers.

1) Uncoordinated Charging: Uncoordinated charging is currently the predominant method of charging EVs throughout the world, as a large percentage of users charge their EVs when they return home. Uncoordinated charging designates that when a user plugs in their EV, charging begins. While this is convenient for EV owners, it may negatively impact the electric grid, for example in equipment overloading or spare capacity absorption as detailed in both of the aforementioned case studies.

2) Coordinated Charging: Coordinated charging is the future direction for EV charging infrastructures. This type of charging is significant for utility providers as they would be able to shape instantaneous energy consumption, in particular the EV charging load, to maintain a desirable load profile at the distribution level and thus ensure high energy efficiency and grid stability [105]. Coordinated charging can also benefit EV owners, by ensuring a reasonable SoC level at times of lower electricity cost as compared to the uncoordinated case [105],[106]. A coordinated charging pilot program was initiated by PG&E and BMW in the state of California from July 2015 to December 2016, called BMW iChargeForward [107]. This pilot program successfully tested the feasibility of managed EV charging as a flexible grid resource, and was a success from the viewpoints of energy reduction as well as customer satisfaction [107].

B. Future Capabilities of OBCs

As EVs become more popular on a global scale, utilities will look to utilize advanced functionalities that OBCs are able to accommodate.

1) Peak Shaving (V2G): One of the well-known and sought-after functionalities for EV OBCs is active V2G power flow control, deemed peak shaving. V2G enables EVs to behave as an energy storage unit that can distribute energy back to the grid whenever required by the utility, typically in a period of high electricity demand. Additionally, EVs can store energy in periods of excess grid-side generation and later deliver it back to the grid, if required [108].

One of the limitations in peak shaving is increased battery degradation, since active power is transferred in both the G2V and V2G operation modes. The effect of daily contributions from both modes has been analyzed in [109]. As expected, battery degradation was pronounced in peak shaving operations primarily due to the high depth-of-discharge requested by the utility. A further limitation for V2G power flow is the power ratings of current OBCs.

2) Ancillary Services (G2V, V2x): While the predominant modes of operation for EV OBCs involve simple G2V and V2G, other smart operations have been identified and investigated [110]. For instance, in [111], additional operational modes include V2H, where the EV is used as a power source for an isolated home or potentially an offline UPS for a grid-connected home, and vehicle-for-grid (V4G), where the EV provides grid support functions, such as reactive power compensation and frequency regulation. A two-stage non-isolated charger exhibiting simultaneous active and reactive power control has been shown in [112], where further it was demonstrated that neither battery lifetime nor SoC were affected by the reactive power support. The same procedure could also be applied to two-stage isolated chargers with the same conclusions, since the front-end PFC stage can take sole responsibility for generating a variable DC link voltage at the requested power factor [113]. One disadvantage is that the two-stage charger will have increased burden on the DC link capacitor, as there will be more charge and discharge cycles compared to only active power control.

Additional to reactive power compensation is grid frequency regulation. In [114], a comprehensive analysis is presented for OBCs providing frequency regulation services as well as the potential impacts on EV battery degradation. As opposed to mechanical systems that take time to react to grid disturbances, EV OBCs could provide more rapid support if controlled appropriately. While EV owners could be paid for offering this service to the grid, based on the presented cost-benefit analysis, it appeared unlikely that financial incentives would be enough, and thus the authors recommend for utilities and government to draft additional motivations. One facet of the second phase of the iChargeForward project aims to investigate engagement strategies to incentivize drivers to participate in V2x programs [107].

While some smart charging techniques and advanced capabilities of OBCs were introduced, an additional point of reference regarding these topics can be found in [110]. Furthermore, a more recent comprehensive overview of smart microgrid control strategies utilizing distributed energy storage (ES) systems is developed in [115]. While [115] applies generally to any ES system, EVs equipped with a bidirectional OBC can be considered as a battery ES system in a smart grid network.

V. Future Trends

A. Trends in Device Utilization

In order to accommodate stringent automotive requirements for high-power OBCs while maintaining compact size and lightweight design, WBG devices, such as SiC and GaN, with fast switching transitions are critical [116],[117]. Tesla recently moved to SiC devices in their chargers and motor drive inverters in the Model 3 [118]. WBG devices and in particular GaN can maintain high charging efficiency at high switching frequency due to their small parasitic capacitances, particularly in the gate- and drain-source [116],[117]. While device paralleling is typically required, a recent study regarding analytical modeling of the parasitics involved in paralleling GaNFETs for applications between 10 kW and 100 kW is published in [119]. The principal benefit of WBG devices operating at high frequency is that passive circuit elements including transformers, inductors, and capacitors can be designed with smaller size and thus the volume and weight of the circuit can be miniaturized. The reduction in passive component size helps to increase the circuit's power density, especially due to reduced system height in the case of planar transformer versus a wound transformer. One example of WBG implementation at high frequency is the DC-DC stage of a 6.6 kW OBC, which utilized GaN devices at 500 kHz switching frequency in [120]. In this converter, an efficiency of >97% and power density of 7.93 kW/L was achieved. An additional example is the DC-DC stage of a 3.3 kW OBC, which utilized GaN devices at 1 MHz switching frequency in **Error! Reference source not found.**. This CLLC-based converter achieved a peak efficiency over 97% and a power density of 9.22 kW/L. A final example is the single-phase, two-stage, 6.6 kW OBC in [122]. The OBC utilizes a critical conduction mode (CRM) interleaved totem-pole boost PFC stage with SiC devices and a switching frequency greater than 300 kHz, and a CLLC-based DC-DC stage with a combination of SiC and GaN devices at ~500 kHz switching frequency. The charger achieves a peak efficiency around 96% and a power density of 2.26 kW/L. WBG technology alongside their opportunities and challenges in automotive applications are detailed in [116]. It is important to note that while the cost of WBG devices is currently quite high, it is projected that the price of SiC and GaN will reduce to $3.32 and $0.54 per device, respectively, by 2022 [123].

B. Trends in Converter Integration

1) Auxiliary Power Module Integrated OBCs: Every EV needs an OBC to charge the high-voltage propulsion battery and an APM to charge the low-voltage auxiliary battery, as shown in Fig. 1. As compared to the propulsion battery, the auxiliary battery is much lower in capacity and voltage level, typically around 12 V. While two independent charging units are currently the industry standard, an OBC integrated with the APM could provide significant weight, size, efficiency, reliability, and cost improvements, since the APM module could be removed from the vehicle entirely as seen in Fig. 9(a). Currently there are no high-power (>7.4 kW) OBCs integrated with the vehicle's APM. Several current EV manufacturers have placed the OBC and APM in the same package, for instance G-power's 3.3 kW and 6.6 kW OBCs with a 1.8 kW DC-DC converter [124],[125]. However, a topological integration has not yet been accomplished at the industry level. With that being said, topological integration has been developed at 3.3 kW in [126] and is the subject of a patent in [127].

The topology utilized is shown in Fig. 9(b) and is comprised of a bidirectional AC-DC PFC converter, a bidirectional half-bridge CLLC DC-DC converter for high voltage battery charging, and a full bridge LLC topology for low voltage charging. The primary, high voltage secondary, and low voltage tertiary sides are integrated using a three-port transformer. The three-port transformer is the heart of this topological integration, and is modeled, designed and optimized in [128]. The transformer presented in [126] has 30 primary turns, 20 secondary turns, and 1 tertiary turn to facilitate the required voltage gains. Furthermore, the leakage inductance is utilized as the resonant inductance to avoid an additional magnetic component in the system. Due to the low voltage and high charging power of the auxiliary battery (12 V, 1 kW), the tertiary side needs to utilize high performance switches to maintain high converter efficiency. Additionally, a bidirectional switch is used to enable the auxiliary battery's charging modes. The prototype charger achieves 94% efficiency.

The operation modes include grid to high voltage battery charging (G2H), grid to low voltage battery charging (G2L), V2G discharging, and high voltage battery to low voltage battery charging (H2L). One significant challenge in OBCs integrated with the APM, is that simultaneous G2H and G2L charging, deemed grid to both battery charging (G2B), is a necessity to enable various functionalities such as battery pre-conditioning, leading to high control complexity. Three-port power flow control algorithms have been previously studied in [129]-[131] for constant voltage and resistive loads; however, three-port power flow between three variable voltage sources is a challenging task, which has not been addressed in the literature. This is due to the fact that alongside simultaneous charging comes the challenge of dual voltage regulation, especially during transient periods, because of the complicated cross-coupled control.

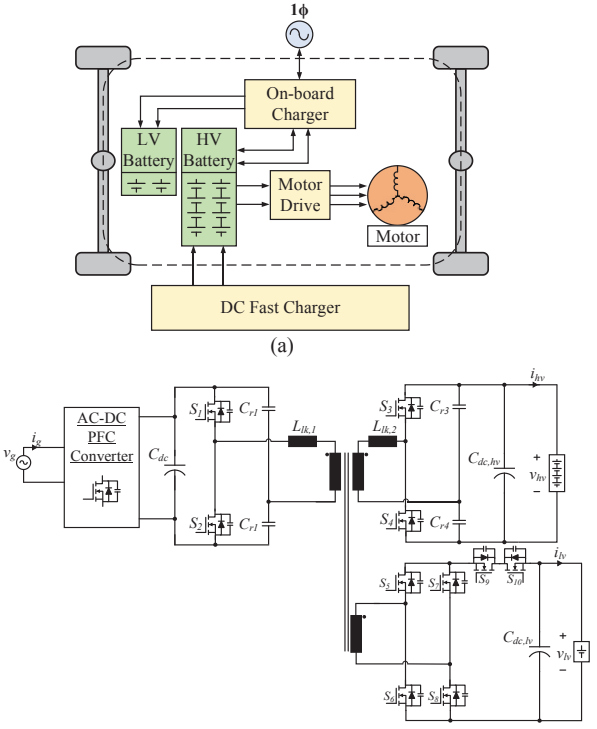

Fig. 9. APM integrated OBC (a) block diagram, and (b) proposed converter topology in [126].

A similar structure to that presented in Fig. 9(b) is researched in [132] with Si devices and [133] with SiC devices. Instead of utilizing an active front-end PFC, the authors propose an additional level of integration with the motor drive inverter. Hence the topology is a combination of the propulsion machine integrated OBC and the APM integrated OBC. The authors mention the capability for operation in G2H, G2B, V2G, and traction mode. However only the G2H mode is verified experimentally, in which the Si prototype achieves a ~94.4% peak efficiency while the SiC iteration achieves a ~96.4% peak efficiency. This system employs the highest level of power electronics integration under current research.

2) Wireless Integrated OBCs: As wireless charging becomes more mature, it is necessary to consider an on-board charging solution that could be compatible with both conductive and inductive charging inputs. The block diagram for a wireless integrated OBC can be seen in Fig. 10. Tesla currently has a patent on wireless integrated charging, where they present two solutions. One solution can operate with conductive and inductive inputs simultaneously, while the other solution only accepts either conductive or inductive charging input at a time [134]. While charging with both conductive and inductive inputs simultaneously is likely not a significant future requirement, it is expected for inductive charging to make more of a future presence for both safety reasons as well as user convenience to charge at rest or while driving [2]. Furthermore, autonomous driving would likely be coupled with autonomous charging, which could be an additional driving force for inductive charging. As one

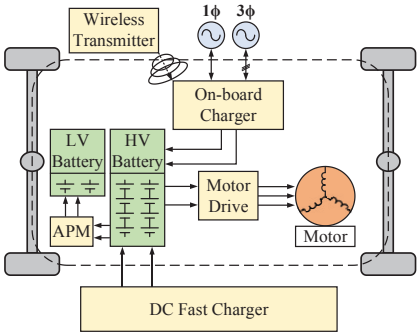

Fig. 10. Wireless integrated OBC block diagram.

example, the future of highway driving may come with toll roads where drivers could wirelessly charge their vehicles while driving [135], which was the subject of two different case studies in [136] and [137]. Therefore, it would be of significant interest to introduce an OBC that with simple modification could accept either grid or wireless inputs for overnight charging, or wireless input for on-road recharging.

One example of such a wireless integrated charger is presented in [138], where the magnetic coupler is integrated with the high frequency transformer of the isolated DC-DC stage of an OBC. In conductive charging mode the novel magnetic coupler acts as an isolation transformer, and in inductive charging mode the coupler acts as a wireless receiver pad. Two different compensation schemes and five designs are comprehensively compared and analyzed for the best design. Furthermore, experimental results at 5 kW demonstrate the magnetic coupler's coupling coefficients in the conductive mode demonstrating behavior similar to an isolation transformer, as well as in the inductive mode with and without coil misalignment. One drawback is that the magnetic coupler's conductive-mode coupling coefficient (~0.93) is still less than the coupling coefficient of a conventional isolation transformer (~0.98), which would lead to a reduction in the circuit's operating efficiency.

3) Integrated Motor Drive and OBC DC-DC Converters: As shown in Fig. 3, a typical OBC is composed of a PFC stage followed by an isolated DC-DC stage. On the other hand, Fig. 11(a) shows the traditional architecture of the motor drive system, which is composed of a DC-DC boost converter to control a fixed or variable DC voltage to the input of the motor-drive inverter. The separate implementation of the OBC and motor drive DC-DC converters results in increased weight and volume of the EV's power electronics, due to large, separate magnetic devices required in the OBC transformer and motor drive DC-DC converter's boost inductors, as well as separate cooling systems.

In order to meet stringent power density targets posed by the U.S. Drive Partnership and EV manufacturers, one method developed in [139] is to integrate the DC-DC converter in the OBC and the motor drive system, shown in Fig. 11(b). The battery contactors present in every EV, shown as S_{11} and S_{12} in Fig. 11(b), enable reconfiguration of the integrated system to utilize one set of magnetics, cooling, and active devices for both charging and motor drive functionalities. In charging

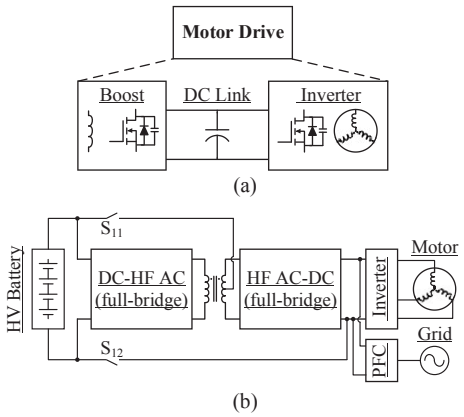

Fig. 11. (a) Typical motor drive block diagram (b) Integrated motor drive and OBC DC-DC converter system [139].

mode the relays are open, and the DC-DC converter is operated as an isolated DAB converter. In traction mode the relays are closed, and the DC-DC converter operates as an interleaved boost converter. A prototype is designed, optimized, and implemented in [139], which integrates the functionality of a 5 kW motor drive interleaved boost converter with a 660 W OBC DAB converter. The prototype is a tenth-scale version of a conventional system enabling 50 kW motor drive and 6.6 kW OBC functionality. The integrated structure achieves a peak efficiency >99% in interleaved boost mode, and >98% in DAB mode, verifying the feasibility and operation principle of the integrated system.

To increase the efficiency of the system in traction mode, particularly in the light-load region, the integrated system can be operated as a DAB instead of an interleaved boost. To accommodate both modes of operation, a mode transition control was developed in [140]. The experimental results verify the control technique and illustrate soft-switching of the battery contactors to minimize degradation and enhance power delivery during a mode transition.

C. Summary and Discussion

As a result of this study on the current state of higher-power conductive-based OBC solution for EVs, several key trends have been identified that could shape the future of EV charging solutions.

1. Increased battery capacity and higher battery voltages will be present in future EVs as auto manufacturers are pushed by government initiatives to reduce emissions, and the need to increase all electric range and enhance vehicle capabilities.

2. Increased charging power level for OBCs will be a future requirement in EVs to maintain, and improve, overnight charging times for higher capacity EVs, and facilitate an infrastructure for faster charging without a significant penetration of level-3 DC fast charging stations.

3. To facilitate high-power OBCs with a higher efficiency and power density, WBG devices including SiC and GaN will be considered in high switching frequency chargers. Furthermore, single-stage chargers and the utilization of integrated planar magnetics will enable high power density OBC designs.

4. Integrated OBCs including propulsion machine, APM and wireless integrated chargers are promising approaches for increasing the power rating of the OBC, while avoiding significant impact on the weight and volume of the charging system.

5. With increasing OBC power ratings, charging will need to be coordinated and controlled. Additionally, OBCs will need to be bidirectional in the future, and compatible with advanced smart grid functionalities. This will not only provide additional OBC functionalities for utilities such as load levelling in V2G, but also for EV owners to use their EV's stored energy.

VI. Conclusion

This manuscript provides a comprehensive overview of high-power (>7.4 kW) conductive-based OBCs for global EVs and the future trends in EV charging. Facilitating higher-power level-2 charging in EVs is the next step in the EV charging industry. This trend is evident because of the projected increase in the EV battery capacity to combat range anxiety, the considerable time and monetary investment required to create an extensive level-3 charging infrastructure, and the fact that level-2 OBC power levels have already doubled over the last five years. To this end, high-power industry-level and research-oriented non-integrated OBCs have been presented and compared, including both modular- and full-power-processing two-stage charging solutions that utilize a DC link capacitor, and single-stage charging solutions that do not utilize a DC link capacitor. Single-stage charging solutions for high-power OBCs may be attractive in order to meet stringent volume, weight, and efficiency constraints posed by EV manufacturers and the U.S. Drive Partnership. Aside from increases in the OBC power rating, charging coordination on the utility side will become a necessity in order to preserve the component power ratings and dynamic performance of the electric grid throughout widespread EV adoption. Furthermore, the functionalities of OBCs are set to expand and include ancillary grid services, alongside controlled V2x power flow. Finally, future trends in the on-board EV power system include the utilization of WBG devices and increased integration, in particular the integration of the OBC with the APM, propulsion system, and/or the wireless charging system.

VII. Acknowledgment

This work has been sponsored partly by the National Science Foundation Grant Numbers, 1602012 and 1507546. which are gratefully acknowledged.

VIII. References

[1] A. Khaligh and S. Dusmez, "Comprehensive Topological Analysis of Conductive and Inductive Charging Solutions for Plug-In Electric Vehicles," in IEEE Transactions on Vehicular Technology, vol. 61, no. 8, pp. 3475-3489, Oct. 2012.

[2] A. Ahmad, M. S. Alam and R. Chabaan, "A Comprehensive Review of Wireless Charging Technologies for Electric Vehicles," in IEEE

Transactions on Transportation Electrification, vol. 4, no. 1, pp. 38-63, March 2018.
[3] Bloomberg New Energy Finance, "Electric Vehicle Outlook 2017," Bloomberg Finance L.P., 2017. [Online]. Available: https://about.bnef.com/electric-vehicle-outlook/
[4] M. A. Hannan, M. M. Hoque, A. Hussain, Y. Yusof and P. J. Ker, "State-of-the-Art and Energy Management System of Lithium-Ion Batteries in Electric Vehicle Applications: Issues and Recommendations," in IEEE Access, vol. 6, pp. 19362-19378, 2018.
[5] International Energy Agency, "Global EV Outlook 2017," IEA Publications, June, 2017. [Online]. Available: https://www.iea.org/publications/freepublications/publication/GlobalEVOutlook2017.pdf
[6] International Energy Agency, "Global EV Outlook 2018," IEA Publications, May 2018. [Online]. Available: https://webstore.iea.org/download/direct/1045?filename=global_ev_outlook_2018.pdf
[7] M. Yilmaz and P. T. Krein, "Review of Battery Charger Topologies, Charging Power Levels, and Infrastructure for Plug-In Electric and Hybrid Vehicles," in IEEE Transactions on Power Electronics, vol. 28, no. 5, pp. 2151-2169, May 2013.
[8] B. M. Conlon, "How Much Capability Do Electric Vehicles Need to Meet Customer Demands? [Viewpoint]," in IEEE Electrification Magazine, vol. 5, no. 1, pp. 4-73, March 2017.
[9] Reuters, "The Number of Electric Cars on the World's Roads Doubled Last Year," Fortune, June 7, 2017. [Online]. Available: http://fortune.com/2017/06/07/2-million-electric-cars/
[10] EVObsession, "Electric Car Sales," 2018. [Online]. Available: https://evobsession.com/electric-car-sales/
[11] Smart USA, "Smart EQ Fortwo," 2018. [Online]. Available: https://www.smartusa.com/models/electric-pure-coupe
[12] Hyundai, "Ioniq Electric," 2018. [Online]. Available: https://www.hyundaiusa.com/ioniq/
[13] Kia, "Soul EV," 2018. [Online]. Available: https://www.kia.com/us/en/vehicle/soul-ev/2018
[14] Renault, "Renault Zoe," 2018. [Online]. Available: https://www.renault.co.uk/vehicles/new-vehicles/zoe.html
[15] Volkswagen, "e-Golf," 2018. [Online]. Available: http://www.vw.com/models/e-golf/
[16] BMW, "BMW i3," 2018. [Online]. Available: https://www.bmwusa.com/vehicles/bmwi/bmw-i3.html
[17] Nissan, "2018 Nissan Leaf," 2018. [Online]. Available: https://www.nissanusa.com/vehicles/electric-cars/leaf.html
[18] Tesla, "Model 3," 2018. [Online]. Available: https://www.tesla.com/model3
[19] Tesla, "Vehicle on-board charger," 2018. [Online]. Available: https://www.tesla.com/support/home-charging-installation?redirect=no
[20] Chevrolet, "Bolt EV," 2018. [Online]. Available: http://www.chevrolet.com/electric/bolt-ev-electric-car
[21] Ford, "2018 Focus Electric," 2018. [Online]. Available: https://www.ford.com/cars/focus/models/focus-electric/
[22] WattEV2Buy, "2017 BAIC EC180 EV," 2017. [Online]. Available: https://wattev2buy.com/electric-vehicles/baic/baic-ec180-ev/
[23] WattEV2Buy, "2018 Chery eQ1 EV," 2018. [Online]. Available: https://wattev2buy.com/electric-vehicles/chery-auto/chery-eq1-ev-electric-car/
[24] WattEV2Buy, "JAC iEV7 EV," 2017. [Online]. Available: https://wattev2buy.com/electric-vehicles/jac-motors-electric-vehicles/jac-iev7/
[25] WattEV2Buy, "JMC E200S EV," 2017. [Online]. Available: https://wattev2buy.com/electric-vehicles/jiangling-motor-corporation-jmc-ev/jmc-e200s-ev-specs-sales-news-pictures-range/
[26] R. Xiong, J. Cao, Q. Yu, H. He and F. Sun, "Critical Review on the Battery State of Charge Estimation Methods for Electric Vehicles," in IEEE Access, vol. 6, pp. 1832-1843, 2018.
[27] S. S. Williamson, A. K. Rathore and F. Musavi, "Industrial Electronics for Electric Transportation: Current State-of-the-Art and Future Challenges," in IEEE Transactions on Industrial Electronics, vol. 62, no. 5, pp. 3021-3032, May 2015.
[28] Power Quality Requirements for Plug-in Vehicle Chargers - Part 1: Requirements, SAE International, Standard J2894, 2011.
[29] Electromagnetic Compatibility (EMC)—Part 3: Limits, IEC61000-3 Documents, 2018.
[30] Quality of Electric Energy Supply Harmonics in Public Supply Network, Standard: SC – GB/T 14549, 1993.
[31] IEEE Recommended Practices and Requirements for Harmonic Control in Electrical Power Systems, IEEE Standard 519, 2014
[32] C. Yao, "Semiconductor Galvanic Isolation Based Onboard Vehicle Battery Chargers", Ph.D. Dissertation in Electrical and Computer Engineering, the Ohio State University, 2018.
[33] IEEE Standard for Interconnection and Interoperability of Distributed Energy Resources with Associated Electric Power Systems Interfaces, IEEE Standard 1547, 2018.
[34] IEEE Guide for Smart Grid Interoperability of Energy Technology and Information Technology Operation with the Electric Power System (EPS), End-Use Applications, and Loads, IEEE Standard 2030, 2011.
[35] Safety of power converters for use in photovoltaic power systems - Part 2: Particular requirements for inverters, IEC Standard 62109-2, 2014.
[36] Standard for Inverters, Converters, Controllers and Interconnection System Equipment for Use With Distributed Energy Resources, UL Standard 1741, 2010.
[37] Technical guideline for electrochemical energy storage system interconnecting with distribution network, NB/T Standard 33015, 2014.
[38] SAE Standard J1772, SAE Electric Vehicle and Plug-in Hybrid Electric Vehicle Conductive Charge Coupler, 2010.
[39] Standard IEC 62196, Plugs, socket-outlets, vehicle connectors and vehicle inlets - Conductive charging of electric vehicles - Part 1, 2, 3, 2014.
[40] SAC Standard GB/T 20234, Connection set of Conductive Charging for Electric Vehicles – Part II and III, 2011.
[41] Phoenix Contact, "Charging technology for E-Mobility - Product overview 2017," Phoenix Contact, 2017. [Online]. Available: https://www.phoenixcontact.com/assets/downloads_ed/global/web_dwl_promotion/52006703_EN_DE_E-Mobility_LoRes.pdf
[42] Continental, "CES 2018: Continental automates charging of electric vehicles and makes them a mobile power bank," Continental, December 13, 2017. [Online]. Available: https://www.continental-corporation.com/en/press/press-releases/2017-12-13-ces-charging-116068.
[43] SAE Standard J3068, Electric Vehicle Power Transfer System Using a Three-Phase Capable Coupler, 2018.
[44] U.S. Department of Energy Office of Energy Efficiency and Renewable Energy, "Enabling Fast Charging: A Technology Gap Assessment", pps. 4-5, October 2017. [Online]. Available: https://www.energy.gov/sites/prod/files/2017/10/f38/XFC%20Technology%20Gap%20Assessment%20Report_FINAL_10202017.pdf.
[45] U.S. Department of Energy Office of Energy Efficiency and Renewable Energy, "Fiscal Year 2018 Advanced Vehicle Technologies Research Funding Opportunity Announcement: DE-FOA-0001919", pp. 6, May 2018. [Online]. Available: https://eere-exchange.energy.gov/FileContent.aspx?FileID=a0948ac6-6da7-4a45-a613-d83688193f1c.
[46] M. A. Hannan, M. M. Hoque, A. Hussain, Y. Yusof and P.J. Ker, "State-of-the-Art and Energy Management System of Lithium-Ion Batteries in Electric Vehicle Applications: Issues and Recommendations," in IEEE Access, vol. 6, pp. 19362-19378, 2018.
[47] Porsche, "Mission E," Porsche Newsroom, July 30, 2018. [Online]. Available: https://newsroom.porsche.com/default/en/products/porsche-taycan-mission-e-drive-unit-battery-charging-electro-mobility-dossier-sportscar-production-christophorus-387-15827.html.
[48] U.S. Drive, "Electrical and Electronics Technical Team Roadmap," Department of Energy, October 2017. [Online]. Available: https://www.energy.gov/sites/prod/files/2017/11/f39/EETT%20Roadmap%2010-27-17.pdf
[49] K. Stengert, "On-board 22 kW fast charger "NLG6"," 2013 World Electric Vehicle Symposium and Exhibition (EVS27), Barcelona, 2013, pp. 1-11.
[50] BRUSA, "NLG664 – On Board Fast Charger," BRUSA, 2018. [Online]. Available: https://www.brusa.biz/fileadmin/template/Support-Center/Datenbl%C3%A4tter/BRUSA_DB_EN_NLG664.pdf
[51] BRUSA, "NLG667 – On Board Fast Charger," BRUSA, 2018. [Online]. Available: http://www.brusa.biz/fileadmin/template/Support-Center/Datenbl%C3%A4tter/BRUSA_DB_EN_NLG667.pdf
[52] G-Power, "10kW air cooled on board charger," G-Power, 2015. [Online]. Available: http://www.gevpower.com/product_detail_en3/id/5.html
[53] Continental, "On-Board Charger," Continental, 2017. [Online]. Available: https://www.continental-automotive.com/en-gl/Passenger-Cars/Powertrain/Electrification/Charging-Technologies/On-Board-Charger

[54] S. Bolte, C. Henkenius, J. Böcker, A. Zibart, E. Kenig and H. Figge, "Water-cooled on-board charger with optimized cooling channel," 2017 19th European Conference on Power Electronics and Applications (EPE'17 ECCE Europe), Warsaw, 2017, pp. P.1-P.9.

[55] H. Wang and F. Blaabjerg, "Reliability of Capacitors for DC-Link Applications in Power Electronic Converters—An Overview," in IEEE Transactions on Industry Applications, vol. 50, no. 5, pp. 3569-3578, Sept.-Oct. 2014.

[56] G. Yang, E. Draugedalen, T. Sorsdahl, H. Liu and R. Lindseth, "Design of High Efficiency High Power Density 10.5kW Three Phase On-board-charger for Electric/hybrid Vehicles," PCIM Europe 2016; International Exhibition and Conference for Power Electronics, Intelligent Motion, Renewable Energy and Energy Management, Nuremberg, Germany, 2016, pp. 1-7.

[57] J. Schmenger, S. Endres, S. Zeltner and M. März, "A 22 kW on-board charger for automotive applications based on a modular design," 2014 IEEE Conference on Energy Conversion (CENCON), Johor Bahru, 2014, pp. 1-6.

[58] F. Musavi, M. Edington, W. Eberle and W. G. Dunford, "Evaluation and Efficiency Comparison of Front End AC-DC Plug-in Hybrid Charger Topologies," in IEEE Transactions on Smart Grid, vol. 3, no. 1, pp. 413-421, March 2012.

[59] J. Lu et al., "A Modular Designed Three-phase High-efficiency High-power-density EV Battery Charger Using Dual/Triple-Phase-Shift Control," in IEEE Transactions on Power Electronics.

[60] N. D. Weise, G. Castelino, K. Basu and N. Mohan, "A Single-Stage Dual-Active-Bridge-Based Soft Switched AC–DC Converter With Open-Loop Power Factor Correction and Other Advanced Features," in IEEE Transactions on Power Electronics, vol. 29, no. 8, pp. 4007-4016, Aug. 2014.

[61] G. Liu et al., "Comparison of SiC MOSFETs and GaN HEMTs based high-efficiency high-power-density 7.2kW EV battery chargers," 2017 IEEE 5th Workshop on Wide Bandgap Power Devices and Applications (WiPDA), Albuquerque, NM, 2017, pp. 391-397.

[62] X. Wang, C. Jiang, B. Lei, H. Teng, H. K. Bai and J. L. Kirtley, "Power-Loss Analysis and Efficiency Maximization of a Silicon-Carbide MOSFET-Based Three-Phase 10-kW Bidirectional EV Charger Using Variable-DC-Bus Control," in IEEE Journal of Emerging and Selected Topics in Power Electronics, vol. 4, no. 3, pp. 880-892, Sept. 2016.

[63] A. Mallik and A. Khaligh, "Control of a Three-Phase Boost PFC Converter Using a Single DC Link Voltage Sensor," IEEE Transactions on Power Electronics, vol. 32, no. 8, pp. 6481-6492, Aug. 2017.

[64] A. Mallik, W. Ding, C. Shi and A. Khaligh, "Input Voltage Sensorless Duty Compensation Control for a Three-Phase Boost PFC Converter," IEEE Transactions on Industry Applications, vol. 53, no. 2, pp. 1527-1537, Mar. 2017.

[65] A. Mallik and A. Khaligh, "A Soft-Switching Strategy for Three-Phase Boost Power Factor Correction Rectifiers," in Proc. IEEE IECON, Florence, Oct. 2016.

[66] P. M. Johnson and K. H. Bai, "A dual-DSP controlled SiC MOSFET based 96%-efficiency 20kW EV on-board battery charger using LLC resonance technology," 2017 IEEE Symposium Series on Computational Intelligence (SSCI), Honolulu, HI, 2017, pp. 1-5.

[67] A. Mallik, W. Ding and A. Khaligh, "A Comprehensive Design Approach to an EMI Filter for a 6-kW Three-Phase Boost Power Factor Correction Rectifier in Avionics Vehicular Systems," in IEEE Transactions on Vehicular Technology, vol. 66, no. 4, pp. 2942-2951, April 2017.

[68] A. Singh, A. Mallik and A. Khaligh, "A Comprehensive Design and Optimization of the DM EMI Filter in a Boost PFC Converter," in IEEE Transactions on Industry Applications.

[69] N. D. Weise, K. K. Mohapatra and N. Mohan, "Universal utility interface for Plug-in Hybrid electric vehicles with vehicle-to-grid functionality," IEEE PES General Meeting, Minneapolis, MN, 2010, pp. 1-8.

[70] D. Varajao, L. M. Miranda, and R. E. Araujo, "AC/DC converter with three to single phase matrix converter, full-bridge AC/DC converter and HF transformer," International Patent Application WO2 016 024 223, Feb. 18, 2016.

[71] D. Varajão, L. M. Miranda, R. E. Araújo and J. P. Lopes, "Power transformer for a single-stage bidirectional and isolated ac-dc matrix converter for energy storage systems," IECON 2016 - 42nd Annual Conference of the IEEE Industrial Electronics Society, Florence, 2016, pp. 1149-1155.

[72] D. Varajão, L. M. Miranda and R. E. Araújo, "Towards a new technological solution for community energy storage," 2014 16th European Conference on Power Electronics and Applications, Lappeenranta, 2014, pp. 1-10.

[73] D. Varajão, R. E. Araújo, L. M. Miranda and J. A. P. Lopes, "Modulation Strategy for a Single-Stage Bidirectional and Isolated AC–DC Matrix Converter for Energy Storage Systems," in IEEE Transactions on Industrial Electronics, vol. 65, no. 4, pp. 3458-3468, April 2018.

[74] N. D. Weise, K. Basu and N. Mohan, "Advanced modulation strategy for a three-phase AC-DC dual active bridge for V2G," 2011 IEEE Vehicle Power and Propulsion Conference, Chicago, IL, 2011, pp. 1-6.

[75] F. Jauch and J. Biela, "Modelling and ZVS control of an isolated three-phase bidirectional AC-DC converter," 2013 15th European Conference on Power Electronics and Applications (EPE), Lille, 2013, pp. 1-11.

[76] P. He and A. Khaligh, "Comprehensive Analyses and Comparison of 1 kW Isolated DC–DC Converters for Bidirectional EV Charging Systems," in IEEE Transactions on Transportation Electrification, vol. 3, no. 1, pp. 147-156, March 2017.

[77] P. He and A. Khaligh, "Design of 1 kW bidirectional half-bridge CLLC converter for electric vehicle charging systems," 2016 IEEE International Conference on Power Electronics, Drives and Energy Systems (PEDES), Trivandrum, 2016, pp. 1-6.

[78] B. Li, Q. Li and F. Lee, "High Frequency PCB Winding Transformer with Integrated Inductors for a Bi-directional Resonant Converter," in IEEE Transactions on Power Electronics.

[79] A. Sankar, A. Mallik and A. Khaligh, "Extended Harmonics Based Phase Tracking for Synchronous Rectification in CLLC converters," in IEEE Transactions on Industrial Electronics.

[80] U. A. Sankar, A. Mallik and A. Khaligh, "Duty compensated reduced harmonic control for a single-phase H-bridge PFC converter," 2018 IEEE Applied Power Electronics Conference and Exposition (APEC), San Antonio, TX, USA, 2018, pp. 1996-2000.

[81] A. Mallik, J. Lu and A. Khaligh, "A Comparative Study Between PI and Type-II Compensators for H-Bridge PFC Converter" in IEEE Transactions on Industry Applications, vol. 54, no. 2, pp. 1128-1135, March-April 2018.

[82] Y. Tang, W. Ding and A. Khaligh, "A bridgeless totem-pole interleaved PFC converter for plug-in electric vehicles," 2016 IEEE Applied Power Electronics Conference and Exposition (APEC), Long Beach, CA, 2016, pp. 440-445.

[83] A. Mallik, J. Lu and A. Khaligh, "Sliding Mode Control of Single Phase Interleaved Totem-Pole PFC for Electric Vehicle Onboard Chargers," in IEEE Transactions on Vehicular Technology.

[84] L. Schrittwieser, M. G. Leibl, M. Haider, F. Thony, J. W. Kolar and T. B. Soeiro, "99.3% Efficient Three-Phase Buck-Type All-SiC SWISS Rectifier for DC Distribution Systems," in IEEE Transactions on Power Electronics.

[85] M. Ashourloo, M. S. Zaman, M. Nasr and O. Trescases, "Opportunities for Leveraging Low-Voltage GaN Devices in Modular Multi-level Converters for Electric-Vehicle Charging Applications," 2018 International Power Electronics Conference (IPEC-Niigata 2018 -ECCE Asia), Niigata, Japan, 2018, pp. 2380-2385.

[86] B. Li, Q. Li and F. C. Lee, "A WBG based three phase 12.5 kW 500 kHz CLLC resonant converter with integrated PCB winding transformer," 2018 IEEE Applied Power Electronics Conference and Exposition (APEC), San Antonio, TX, 2018, pp. 469-475.

[87] Briane, B., Loudot, S.: 'Rapid reversible charging device for an electric vehicle'. US Patent No. US 2011/0254494 A1, 2011.

[88] Loudot, S., Briane, B., Ploix, O., et al.: 'Fast charging device for an electric vehicle'. US Patent No. US 2012/0286740 A1, 2013.

[89] S. D. Mohamed, A. A. Elserougi, A. S. Abdel-Khalik, A. M. Massoud, and S. Ahmed, "A nine-switch-converter-based integrated motor drive and battery charger system for EVs using symmetrical six-phase machines," IEEE Trans. Ind. Electron., vol. 63, no. 9, pp. 5326–5335, Sep. 2016.

[90] S. Lacroix, E. Laboure, and M. Hilairet, "An integrated fast battery charger for electric vehicle," in Proc. 2010 IEEE Veh. Power Propulsion Conf., Lille, France, 2010, pp. 1–6.

[91] S. Q. Ali, D. Mascarella, G. Joos, T. Coulombe, and J. M. Cyr, "Three phase high power integrated battery charger for plugin electric vehicles," in Proc. 2015 IEEE Veh. Power Propulsion Conf., Oct. 2015, pp. 1–6.

[92] I. Subotic, N. Bodo, E. Levi, and M. Jones, "Onboard integrated battery charger for EVs using an asymmetrical nine-phase machine," IEEE Trans. Ind. Electron., vol. 62, no. 5, pp. 3285–3295, May 2015.

[93] I. Subotic, N. Bodo, E. Levi, M. Jones, and V. Levi, "Isolated chargers for EVs incorporating six-phase machines," IEEE Trans. Ind. Electron., vol. 63, no. 1, pp. 653–664, Jan. 2016.

[94] I. Subotic, N. Bodo, and E. Levi, "An EV drive-train with integrated fast charging capability," IEEE Trans. Power Electron., vol. 31, no. 2, pp. 1461–1471, Feb. 2016.

[95] C. Shi, Y. Tang and A. Khaligh, "A Three-Phase Integrated Onboard Charger for Plug-In Electric Vehicles," in IEEE Transactions on Power Electronics, vol. 33, no. 6, pp. 4716-4725, June 2018.

[96] A. Khaligh, Y. Tang, and C. Shi, Integrated Onboard Chargers, University of Maryland Invention Disclosure Number PS-2014-127, Provisional Patent Application Numbers 62/059,328 (Oct. 3, 2014) & 62/237,205 (Oct. 5, 2015), U.S. Patent Application No. 15/285,062, filed on Oct. 4, 2016.

[97] I. Subotic, N. Bodo, and E. Levi, "Single-phase on-board integrated battery chargers for EVs based on multiphase machines," IEEE Trans. Power Electron., vol. 31, no. 9, pp. 6511–6523, Sep. 2016.

[98] I. Subotic, N. Bodo, E. Levi, B. Dumnic, D. Milicevic and V. Katic, "Overview of fast on-board integrated battery chargers for electric vehicles based on multiphase machines and power electronics," in IET Electric Power Applications, vol. 10, no. 3, pp. 217-229, 3 2016.

[99] C. Shi and A. Khaligh, "A Two-Stage Three-Phase Integrated Charger for Electric Vehicles with Dual Cascaded Control Strategy," in IEEE Journal of Emerging and Selected Topics in Power Electronics, vol. 6, no. 2, pp. 898-909, June 2018.

[100] C. Shi, Y. Tang and A. Khaligh, "A Single-Phase Integrated Onboard Battery Charger Using Propulsion System for Plug-in Electric Vehicles," in IEEE Transactions on Vehicular Technology, vol. 66, no. 12, pp. 10899-10910, Dec. 2017.

[101] J. Ye, C. Shi and A. Khaligh, "Single-Phase Charging Operation of a Three-Phase Integrated Onboard Charger for Electric Vehicles," 2018 IEEE Transportation Electrification Conference and Expo (ITEC), Long Beach, CA, 2018, pp. 681-686.

[102] C. Saber, D. Labrousse, B. Revol and A. Gascher, "Challenges Facing PFC of a Single-Phase On-Board Charger for Electric Vehicles Based on a Current Source Active Rectifier Input Stage," in IEEE Transactions on Power Electronics, vol. 31, no. 9, pp. 6192-6202, Sept. 2016.

[103] E. Voumvoulakis, E. Leonidaki, G. Papoutsis and N. Hatziargyriou, "Evaluation of the impact of plug-in electric vehicles in Greek distribution network," in CIRED - Open Access Proceedings Journal, vol. 2017, no. 1, pp. 2270-2274, 10 2017.

[104] M. A. Awadallah, B. N. Singh and B. Venkatesh, "Impact of EV Charger Load on Distribution Network Capacity: A Case Study in Toronto," in Canadian Journal of Electrical and Computer Engineering, vol. 39, no. 4, pp. 268-273, Fall 2016.

[105] B. Sun, Z. Huang, X. Tan and D. H. K. Tsang, "Optimal Scheduling for Electric Vehicle Charging With Discrete Charging Levels in Distribution Grid," in IEEE Transactions on Smart Grid, vol. 9, no. 2, pp. 624-634, March 2018.

[106] A. Ahmadian, M. Sedghi, B. Mohammadi-ivatloo, A. Elkamel, M. Aliakbar Golkar and M. Fowler, "Cost-Benefit Analysis of V2G Implementation in Distribution Networks Considering PEVs Battery Degradation," in IEEE Transactions on Sustainable Energy, vol. 9, no. 2, pp. 961-970, April 2018.

[107] S. Kaluza, D. Almeida, and P. Mullen, "BMW i ChargeForward: PG&E's Electric Vehicle Smart Charging Pilot," December 2016 [Online]. Available: http://www.pgecurrents.com/wp-content/uploads/2017/06/PGE-BMW-iChargeForward-Final-Report.pdf

[108] F. Un-Noor, P. Sanjeevikumar, L. Mihet-Popa, and E. Hossain, "A Comprehensive Study of Key Electric Vehicle (EV) Components, Technologies, Challenges, Impacts, and Future Direction of Development," in Energies 10 (8), August 2017.

[109] M. Jafari, A. Gauchia, S. Zhao, K. Zhang and L. Gauchia, "Electric Vehicle Battery Cycle Aging Evaluation in Real-World Daily Driving and Vehicle-to-Grid Services," in IEEE Transactions on Transportation Electrification, vol. 4, no. 1, pp. 122-134, March 2018.

[110] M. Yilmaz and P. T. Krein, "Review of the Impact of Vehicle-to-Grid Technologies on Distribution Systems and Utility Interfaces," in IEEE Transactions on Power Electronics, vol. 28, no. 12, pp. 5673-5689, Dec. 2013.

[111] V. Monteiro, J. G. Pinto and J. L. Afonso, "Operation Modes for the Electric Vehicle in Smart Grids and Smart Homes: Present and Proposed Modes," in IEEE Transactions on Vehicular Technology, vol. 65, no. 3, pp. 1007-1020, March 2016.

[112] M. C. Kisacikoglu, M. Kesler and L. M. Tolbert, "Single-Phase On-Board Bidirectional PEV Charger for V2G Reactive Power Operation," in IEEE Transactions on Smart Grid, vol. 6, no. 2, pp. 767-775, March 2015.

[113] M. Restrepo, J. Morris, M. Kazerani and C. A. Cañizares, "Modeling and Testing of a Bidirectional Smart Charger for Distribution System EV Integration," in IEEE Transactions on Smart Grid, vol. 9, no. 1, pp. 152-162, Jan. 2018.

[114] A. O. David and I. Al-Anbagi, "EVs for frequency regulation: cost benefit analysis in a smart grid environment," in IET Electrical Systems in Transportation, vol. 7, no. 4, pp. 310-317, 12 2017.

[115] T. Morstyn, B. Hredzak and V. G. Agelidis, "Control Strategies for Microgrids With Distributed Energy Storage Systems: An Overview," in IEEE Transactions on Smart Grid, vol. 9, no. 4, pp. 3652-3666, July 2018.

[116] D. Han, S. Li, W. Lee and B. Sarlioglu, "Adoption of wide bandgap technology in hybrid/electric vehicles-opportunities and challenges," 2017 IEEE Transportation Electrification Conference and Expo (ITEC), Chicago, IL, 2017, pp. 561-566.

[117] H. A. Mantooth, M. D. Glover, and P. Shepherd, "Wide bandgap technologies and their implications on miniaturizing power electronic systems," IEEE J. Emerg. Sel. Topics Power Electron, vol. 2, no. 3, pp. 374–385, Sep. 2014.

[118] S. Bakker, "Tesla Model 3 Powertrain Fun.," Clean Technica, May 28, 2018. [Online]. Available: https://cleantechnica.com/2018/05/28/more-tesla-model-3-powertrain-fun-from-carburetors-to-carborundum-youve-come-a-long-way-baby/

[119] J. L. Lu and D. Chen, "Paralleling GaN E-HEMTs in 10kW–100kW systems," 2017 IEEE Applied Power Electronics Conference and Exposition (APEC), Tampa, FL, 2017, pp. 3049-3056.

[120] B. Li, Q. Li and F. C. Lee, "A novel PCB winding transformer with controllable leakage integration for a 6.6kW 500kHz high efficiency high density bi-directional on-board charger," 2017 IEEE Applied Power Electronics Conference and Exposition (APEC), Tampa, FL, 2017, pp. 2917-2924.

[121] P. He, A. Mallik, A. Sankar and A. Khaligh, "Design of a 1-MHz High-Efficiency High-Power-Density Bidirectional GaN-Based CLLC Converter for Electric Vehicles," in IEEE Transactions on Vehicular Technology, vol. 68, no. 1, pp. 213-223, Jan. 2019.

[122] B. Li, Q. Li, F. C. Lee, Z. Liu and Y. Yang, "A High-Efficiency High-Density Wide-Bandgap Device-Based Bidirectional On-Board Charger," in IEEE Journal of Emerging and Selected Topics in Power Electronics, vol. 6, no. 3, pp. 1627-1636, Sept. 2018.

[123] US Department of Energy, "Wide Bandgap Power Electronics Technology Assessment", pp. 11, Feb. 2015. [Online]. Available: https://www.energy.gov/sites/prod/files/2015/02/f19/QTR%20Ch8%20-%20Wide%20Bandgap%20TA%20Feb-13-2015.pdf.

[124] G-Power, "3.3KW OBC + 1.8KW DCDC," G-Power, 2015. [Online]. Available: http://www.gevpower.com/product_detail_en5/id/8.html

[125] G-Power, "6.6kW OBC + 1.8KW DCDC," G-Power, 2015. [Online]. Available: http://www.gevpower.com/product_detail_en5/id/9.html

[126] Y. Tang, J. Lu, B. Wu, S. Zou, W. Ding and A. Khaligh, "An Integrated Dual-Output Isolated Converter for Plug-in Electric Vehicles," in IEEE Transactions on Vehicular Technology, vol. 67, no. 2, pp. 966-976, Feb. 2018.

[127] A. Khaligh and Y. Tang, An Integrated Dual-Output Grid-to-Vehicle (G2V) and Vehicle-to-Grid (V2G) Onboard Charger for Plug-In Electric Vehicles, University of Maryland Invention Disclosure Number PS-2013-055, Provisional Patent Application No. 62/011649, U.S. Patent Application No. 14/739,822, PCT Patent Application No. PCT/US15/35837, filed on Jun. 15, 2015.

[128] S. Zou, J. Lu, A. Mallik and A. Khaligh, "Modeling and Optimization of an Integrated Transformer for Electric Vehicle On-Board Charger Applications," in IEEE Transactions on Transportation Electrification, vol. PP, no. 99, pp. 1-1.

[129] C. Zhao, S. D. Round and J. W. Kolar, "An Isolated Three-Port Bidirectional DC-DC Converter With Decoupled Power Flow Management," in IEEE Transactions on Power Electronics, vol. 23, no. 5, pp. 2443-2453, Sept. 2008.

[130] H. Tao, A. Kotsopoulos, J. L. Duarte and M. A. M. Hendrix, "Transformer-Coupled Multiport ZVS Bidirectional DC–DC Converter With Wide Input Range," in IEEE Transactions on Power Electronics, vol. 23, no. 2, pp. 771-781, March 2008.

[131] B. Karanayil, M. Ciobotaru and V. G. Agelidis, "Power Flow Management of Isolated Multiport Converter for More Electric

Aircraft," in IEEE Transactions on Power Electronics, vol. 32, no. 7, pp. 5850-5861, July 2017.

[132] G. Su and L. Tang, "A new integrated onboard charger and accessory power converter for plug-in electric vehicles," 2014 IEEE Energy Conversion Congress and Exposition (ECCE), Pittsburgh, PA, 2014, pp. 4790-4796.

[133] G. Su and L. Tang, "An integrated onboard charger and accessory power converter for traction drive systems with a boost converter," 2016 IEEE Energy Conversion Congress and Exposition (ECCE), Milwaukee, WI, 2016, pp. 1-6.

[134] T. Nergaard and J. Straubel, Integrated Inductive and Conductive Electrical Charging System, United States Patent 8,933,661, Jan. 15, 2015.

[135] T. E. Stamati and P. Bauer, "On-road charging of electric vehicles," 2013 IEEE Transportation Electrification Conference and Expo (ITEC), Detroit, MI, 2013, pp. 1-8.

[136] M. Taljegard, L. Thorson, M. Odenberger and F. Johnsson, "Electric road systems in Norway and Sweden-impact on CO2 emissions and infrastructure cost," 2017 IEEE Transportation Electrification Conference and Expo, Asia-Pacific (ITEC Asia-Pacific), Harbin, 2017, pp. 1-6.

[137] A. Shekhar, M. Bolech, V. Prasanth and P. Bauer, "Economic considerations for on-road wireless charging systems - A case study," 2015 IEEE PELS Workshop on Emerging Technologies: Wireless Power (2015 WoW), Daejeon, 2015, pp. 1-5.

[138] E. G. Marques, S. V. da Silva and A. M. S. Mendes, "A new magnetic coupler for EVs chargers based on plug-in and IPT technologies," 2017 IEEE Energy Conversion Congress and Exposition (ECCE), Cincinnati, OH, 2017, pp. 2760-2766.

[139] S. Anwar, W. Zhang, F. Wang and D. J. Costinett, "Integrated DC-DC converter design for Electric Vehicle powertrains," 2016 IEEE Applied Power Electronics Conference and Exposition (APEC), Long Beach, CA, 2016, pp. 424-431.

[140] S. Anwar and D. J. Costinett, "Operating mode transition control of a SiC integrated DC DC powertrain charger for electric vehicles," 2017 IEEE Transportation Electrification Conference and Expo (ITEC), Chicago, IL, 2017, pp. 152-157.